A Reanalysis of the Diverse Sodium Species in Carbon Anodes for Sodium Ion Batteries: A Thermodynamic View

Zhihong Tian, Yu Zhang,* Jixin Zhu, Qiuye Li, Tianxi Liu, and Markus Antonietti*

Sodium ion batteries (SIBs) have been extensively investigated as a promising alternative for lithium ion batteries (LIBs) owing to the readily available character of sodium, lower costs of battery systems, as well as a similar working mechanism to LIBs. However, this view turns out to be oversimplified; countless reviews especially in the last years contradict each other, and it is still a challenging task to design highly performing electrode materials for SIBs. Due to the larger radius of Na^+, its lower covalent character, and the resulting changes in intercalation chemistry, sodium is far from being only the bigger relative of lithium, and the difference leads to altered loading curves, and the occurrence of a multiplicity of binding sites. An in-depth holistic understanding of the sodium storage mechanisms is needed to resolve the controversial discussions in the research community, ideally starting with unquestionable thermodynamic points. Here, taking a tutorial perspective, first the recent discussions on the storage mechanism of sodium in carbons are reviewed from an unorthodox viewpoint, namely addressing sodium uptake as a multifaceted adsorption process with an added electrochemical binding potential. This model is based on literature data. Afterward, challenges and perspectives revealed by such a model are discussed.

1. Introduction

The quest for a more economic and efficient utilization of renewable electricity sources such as solar, wind, and tidal energy has moved the technological bottleneck to cheap and more sustainable energy storage systems.[1–5] Rechargeable lithium-ion batteries (LIBs) as one of the state-of-the-art electricity storage technologies are omnipresent in portable electronic devices and electric vehicles due to their comparably high energy density and low self-discharge rate,[6–8] but the high-cost and insufficient lithium resources seriously bias grid applications.[9] Such considerations made sodium ion batteries (SIBs) emerge, which is due to the abundance, low cost, and simple access of sodium.[10–17] However, the larger radius of Na^+ relative to Li^+ changes the rules of ion intercalation seriously, for example, Na cannot intercalate into graphite. To this end, advanced electrode materials, especially suitable anode materials, were, but still have to be developed for making the SIB performance competetive.[18–20]

Carbon-based materials are in principle always a good choice with favorable features such as low cost, abundance, and stability. Graphite as a commercialized anode in LIBs is for Na, almost thermodynamically unaccessible,[21,22] while binding of solvated Na^+ ions comes mostly with a lower storage capacity (about half of that for LIBs).[23,24] So-called hard carbons with defects and voids have been identified as the most promising anode materials with favorable capacities exceeding 300 mAh g^{-1} and can be considered as state-of-the-art.[25–29] Further enhancement of hard carbons can be achieved via heteroatom doping including nitrogen, oxygen, or sulfur, improving the electric

Z. Tian, Q. Li
Engineering Research Center for Nanomaterials
Henan University
Kaifeng 475004, P. R. China
Z. Tian, M. Antonietti
Department of Colloid Chemistry
Max Planck Institute of Colloids and Interfaces
14476 Potsdam, Germany
E-mail: office.cc@mpikg.mpg.de

The ORCID identification number(s) for the author(s) of this article can be found under https://doi.org/10.1002/aenm.202102489.

Y. Zhang
School of Mechanical and Power Engineering
East China University of Science and Technology
Shanghai 200237, P. R. China
E-mail: yzhang071@ecust.edu.cn
J. Zhu
Institute of Advanced Materials (IAM)
Nanjing Tech University
Nanjing 211816, P. R. China
T. Liu
Key Laboratory of Synthetic and Biological Colloids
Ministry of Education
School of Chemical and Material Engineering
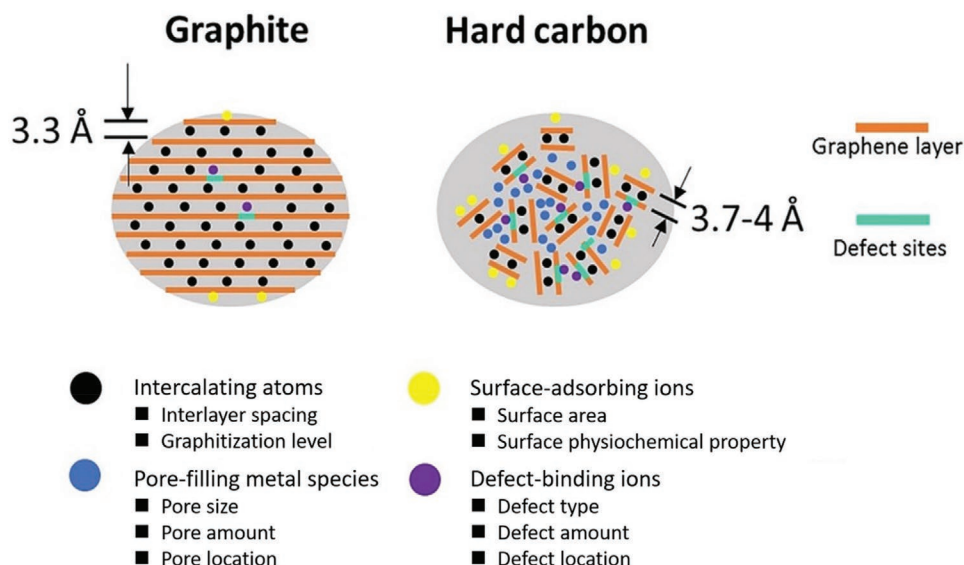Jiangnan University
Wuxi 214122, P. R. China

Figure 1. Schematic illustration of the differences in structure and charge/atom storage between the graphite and hard carbon. Reproduced with permission.[50] Copyright 2018, Wiley-VCH.

conductivity, and breaking graphitic packing.[30–32] The overall performance is, however, still not remarkable, and to achieve high capacity, stable cycling, and high Coulombic efficiency (CE) simultaneously from the first cycle is very difficult. Therefore, an in-depth understanding of the interaction processes toward the sodium storage in hard carbon-based anodes is highly profitable and in our opinion, the most promising way to resolve the current contradictious situation.

There has been already a larger number of papers reviewing the advances of electrode materials for SIBs, and we advise to read some of them as they mark the missing understanding of effects and interactions in complex materials as such.[33–41] Others, as discussed below in detail, assign the different phases of sodium storage in an exactly opposing way, and only one of them can of course be correct, and the unresolved contradictions confuse especially people who newly enter this relevant field. Motivated by our own research on carbon materials, we will try to address these problems by discussing the electrochemical sodium storage only as a special interaction process, however complying with a general thermodynamic and molecular perspective of sorption processes in carbon. Using the Nernst equation as a transcript, we transform electrochemical curves into sorption phenomena and relate those phenomena to the structure of carbons in well-established chemical model systems. Based on the thermodynamic interpretation, then, an updated picture for the rather complex processes in hard carbon SIBs is proposed. Such a model will help to optimize the diverse effects independently, for the sake of better performing and more stable SIBs. The understanding of such interaction processes can then be potentially extended to other rechargeable battery systems using redox carriers such as K, Mg, Ca, and Al, and also to other ion/carbon interactions such as ion sorption, purification, and catalysis.[42–44] Finally, our perspectives on the unresolved challenges and future research issues are also provided.

2. Current Status of Fundamental Sodium Storage Mechanism

Carbon materials are promising electrode materials due to their excellent electrochemical stability and cost effectiveness.[45] Particularly, for SIBs, hard (non-graphitizable) carbon with defects, micro-voids, as well as large interlayer spacings (>0.37 nm) have been reported to possess high reversible capacities exceeding 300 mAh g^{-1}, which is comparable to the theoretical specific capacity of graphite (372 mAh g^{-1}) in the commercial LIB anode.[46–49] Different from the periodic stacking of graphene layers with a spacing of 3.3 Å, hard carbon shows randomly distributed graphene layers with expanded interlayer spacing and sub-nanometer slit pores between the covalent layers (**Figure 1**).[50] For graphite, the lithium storage is mainly based on the intercalation between the graphene layers, while hard carbon has diverse types of sites and binding, including the intercalation, the storage in micropores, and adsorption onto defects and at the surface. Different to the well-established storage mechanism of Li in graphite, the sodium insertion mechanism in hard carbon is partly ionic, partly adsorptive, and still controversially discussed. Hard carbon suffers from low initial coulombic efficiency (ICE) and unsatisfactory rate capabilities due to the severe side reactions such as the electrolyte decomposition and poor ion diffusion kinetics.[51–53] Therefore, the fundamental understanding of the interaction at a molecular scale during sodium storage plays a key role in providing a more effective guideline to the rational design of high-performance carbon-based anodes.

Up to now, hard carbon is generally synthesized through pyrolysis of polymers, biomass or sugar, during which randomly packed single graphitic layers are formed.[54–56] It should be noted that a wide range of precursors were used, and the detailed and systematic analysis of the effect of chemical choices on the structure of hard carbon is still missing. For example, diverse biomass sources such as lotus stem, peat, or
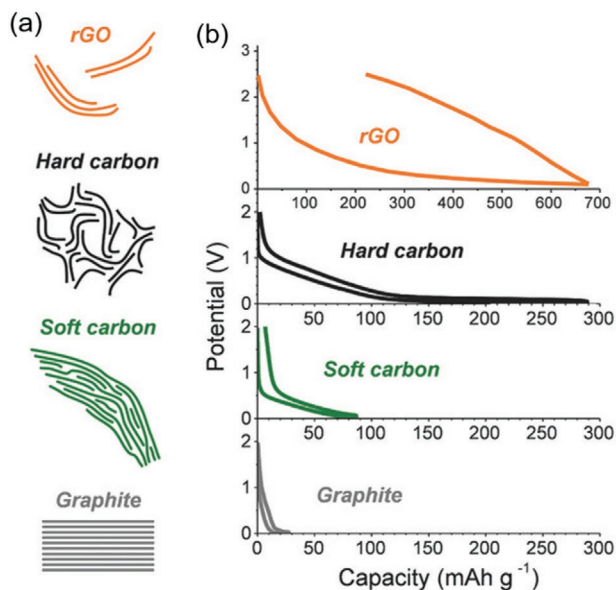
ADVANCED
SCIENCE NEWS
www.advancedsciencenews.com

ADVANCED
ENERGY
MATERIALS
www.advenergymat.de

Figure 2. a) Schematic representation of the local carbon architectures. b) Typical voltage–charge profiles at second cycle in sodium half-cell of reduced graphite oxide, hard carbon (black), soft carbon (green), and graphite (grey). Reproduced with permission.[62] Copyright 2018, Wiley-VCH.

pinecone have been pyrolyzed to achieve hard carbon resulting in different pore structures and/or doped elements.[57–59] The chemical nature of the precursors has indeed a complex effect on the microstructure, texture, and the content and type of heteroatoms of the as-generated hard carbon, leading to a difficult correlation to the structure and sodium storage behavior. Furthermore, the type of electrolyte also affects the electrochemical behavior, that is, certain carbons behave differently in different solvents.[60,61] The typical voltage–capacity discharging profile of hard carbon is shown in **Figure 2** and consists of at least one or two sloping regions (0.1–2.0 V, vs Na^+/Na) and a plateau region (below 0.1 V, vs Na^+/Na). The high capacity and high voltage of hard carbons as compared to soft carbons or graphite can be ascribed to a longer voltage plateau.[62]

There are many reports on how to assign the different voltage regions to different structures and different processes, and as mentioned, the situation is at least controversial. In 2000, Stevens and Dahn first proposed an "intercalation-filling" mechanism for the sodium storage behavior of hard carbon with a "house of cards" structure (cards randomly depositing onto each other).[26,63,64] They demonstrated that the capacity from the slope region is mainly ascribed to the integration of Na^+ ions onto special graphene sites, while the plateau region reflects the filling/plating of metallic Na into the nanopores (**Figure 3**a). Similar results were later obtained by Komaba et al. with the evidence that the Bragg peak at 23.4° was shifted to a lower angle during the discharging process to 0.1 V, indicating graphitic layer expansion by turning Na^0 into Na^+.[65] A red shift of G-band in Raman spectroscopy in the sloping region while no shift in the plateau region further confirmed that Na^+ structurally integrated in the sloping region.

Apparently incompatible with the "intercalation-filling" mechanism, Tarascon et al. proposed an "adsorption-filling"
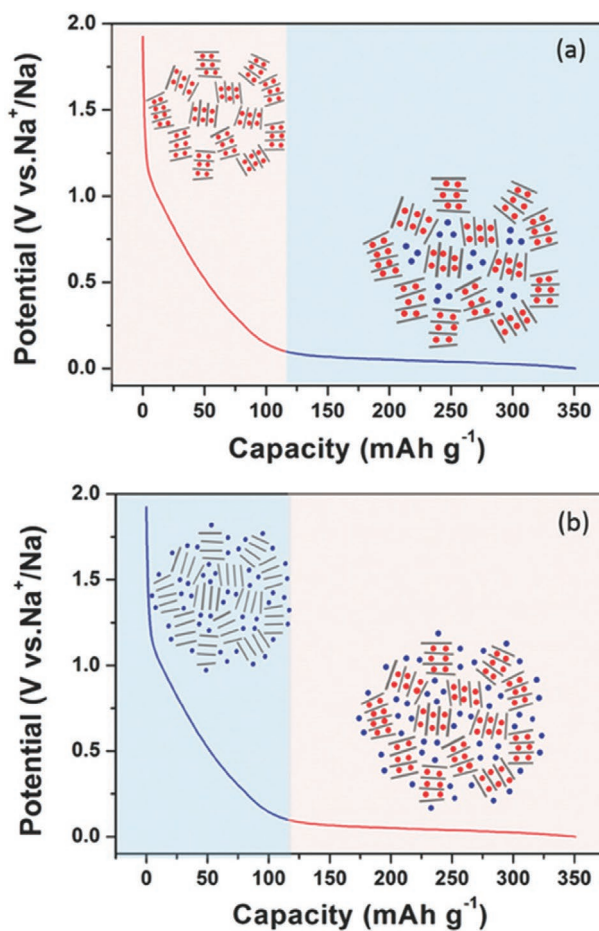

Figure 3. Schematic illustration of the mechanisms for Na-ion storage in hard carbon. a) "Intercalation–adsorption" mechanism. b) "Adsorption–intercalation" mechanism. Reproduced with permission.[70] Copyright 2017, Wiley-VCH.

mechanism for the first sloping region above 1.0 V given by the energetics of Na^+ adsorption onto defects, the second sloping region (0.1–1.0 V) for a Na^+ adsorption onto carbon sites, and the plateau region for "nanopore filling" with metallic Na.[66] This idea was supported by the observation that the plateau vanished when the micropores of hard carbon were filled with sulfur.[67] We add here for better understanding that any Na^+ uptake represents an electrochemical capacity and must come with an extra electron stored in the conjugated carbon, that is, a Na^+/e^- pair is stored and thereby the process is similar to a supercapacitor. The mutual repellence of the electrons within the carbon pool also explains the sloping as such, as Coulomb law then dictates that more charges can only be integrated at higher potentials, in the ideal case with a triangular "sloping" profile. In nice agreement with these explanations, the slope region capacity decreased when the hard carbon was prepared at a higher pyrolysis temperature and thus reduced concentration of defects, indicative for the type of adsorption sites reflected in this region.

The "adsorption-filling" mechanism was afterward critically and partly passionately questioned by many other groups. In particular, according to this mechanism, the specific capacities
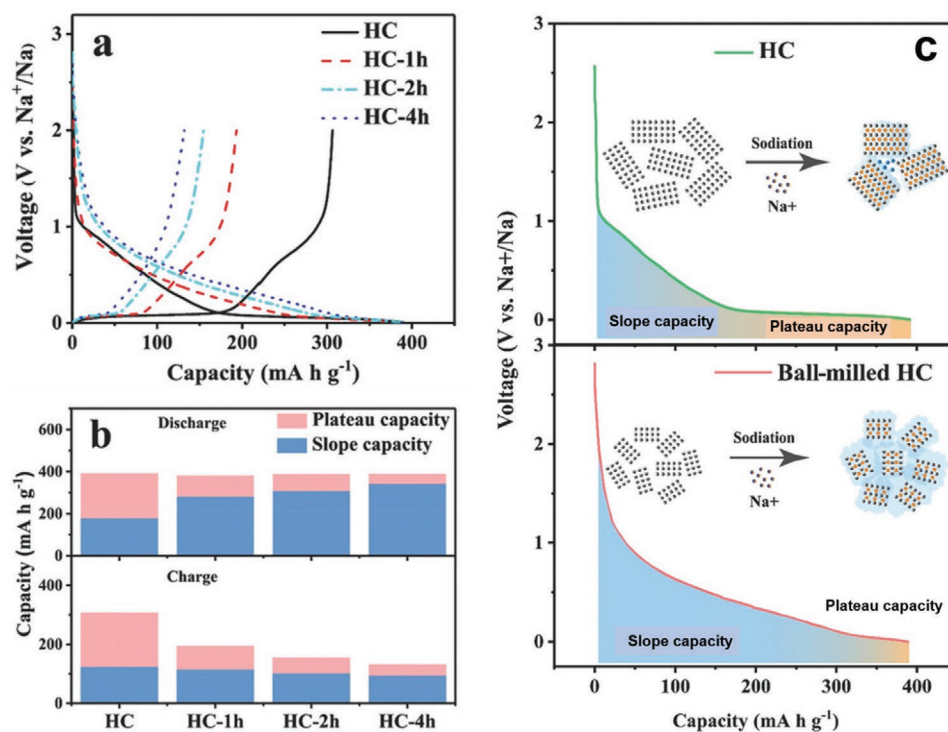
**ADVANCED
SCIENCE NEWS**

www.advancedsciencenews.com

**ADVANCED
ENERGY
MATERIALS**

www.advenergymat.de

Figure 4. Electrochemical performance of the hard carbon electrodes. a) The initial galvanostatic charge–discharge curves of the hard carbon electrodes at a current rate of 20 mA g^{-1}. b) Summary of the capacity distribution during the charge and discharge process at a current rate of 20 mA g^{-1}. c) Schematic illustration of the sodiation process of the HC and ball-milled HC. Reproduced with permission.[75] Copyright 2018, Wiley-VCH.

from the plateau region should be positively related to the pore volume of hard carbon, while no clear correlation was found. For example, a hard carbon prepared at a low temperature of <1000 °C possessed abundant micropores, while no plateau capacity could be observed.[68,69] This asks for a further refinement of the notation "micropore" to be explained later in this article, that is, what type of micropore interaction really can contribute to store Na(0).

An "adsorption–intercalation" mechanism was proposed by Cao et al., which again ascribes the sloping region to the Na$^+$ adsorption on the carbon surface, while the plateau region is now due to the Na intercalation between the expanded graphene layers (Figure 3b).[71] Currently, this model has been supported by the work of many different groups.[72–74] Based on the ex situ X-ray diffraction, a reversible expansion/contraction of the (002) d-spacing in the plateau region can be detected, which clearly supports Na intercalation into the graphene layers. To reveal further details of this mechanism, Cao et al. prepared a series of cellulose-based hard carbons with different concentrations of defects through extending ball-milling time and then investigated their performance in dependence of the structure.[75] **Figure 4**a shows their initial galvanostatic charge–discharge curves at a current density of 20 mA g^{-1}. It was found that the initial discharge capacities were almost the same, while the initial coulombic efficiency (ICE) decreased with the increasing ball-milling time (i.e., the increasing concentration of defects). Furthermore, according to Figure 4b, the slope capacity sharply increased from 178.3 mAh g^{-1} for HC to 342.3 mAh g^{-1} for HC-4h (hard carbon subjected to 4 h of ball milling), while the plateau capacity severely decreased from 213 mAh g^{-1} for HC to

46.4 mAh g^{-1} for HC-4h for the discharging process. These data obviously contradict the "intercalation-filling" mechanism, as a larger pore volume of the hard carbon created by longer ball-milling time should enable higher "filling". On the other hand, these data are well explained by the "adsorption–intercalation" mechanism as a hard carbon with longer ball-milling time and thus more defects resulted in less sites for Na within ordered layer stacks. The higher slope capacity relative to those of other hard carbons with short ball-milling time can then be ascribed to the presence of edges and surface defects, which provided active adsorption sites for Na$^+$, but also led to higher ICE. To illustrate this scenario in a simple scheme, Figure 4c shows the comparison of the sodium storage behaviors of hard carbon with and without ball milling.

Furthermore, the sodium storage behavior of hard carbon was also investigated using several electrochemical techniques, including cyclic voltammetry (CVs) and galvanostatic intermittent titration (GITT) to reveal the reaction kinetics.[76] For example, Wu et al. investigated the sodium storage mechanism of a free-standing hard carbon paper derived from a commercial carbon tissue in an ether electrolyte.[77] As shown in **Figure 5**a, the CV curves tested at varied scan rates showed two pairs of representative peaks marked as P/P' at a low potential and S/S' at a high potential, respectively. Typically, the peak current (i) and scan rate (v) of the CV curves follow the equation: $i = av^b$, which can be transformed into the equation: $\log(i) = b \times \log(v) + \log(a)$, where a and b are the adjustable parameters. Through fitting the results, one can determine the electrochemical reaction is surface-controlled (b close to 1) or diffusion-controlled (b close to 0.5). As shown in Figure 5b,
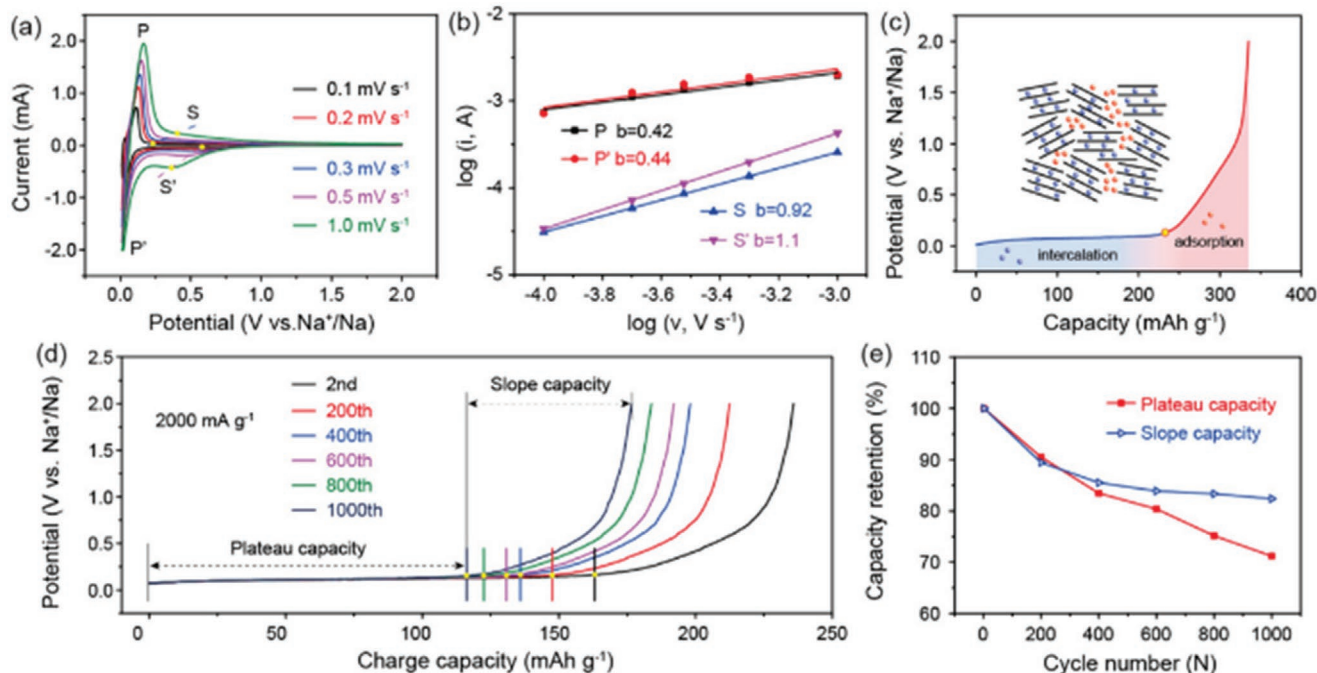
2102489 (4 of 17)

Figure 5. Analyses for the electrochemical data of HCP electrode in ether electrolyte. a) CV curves at varied scan rates from 0.1 to 1.0 mV s^{-1}. b) Plots of log(i) versus log(v) and the corresponding linear fitting. c) Schematic illustration of sodium storage mechanism. d) Charge curves at different cycles at 2000 mA g^{-1}. e) Statistical results of plateau and slope capacity in (d). Reproduced with permission.[77] Copyright 2019, Wiley-VCH.

the values of b for P/P' and S/S' were 0.42/0.44 and 0.92/1.10, respectively, indicating that the plateau region below 0.2 V (corresponding to the range of P'/P peaks in CV) represents the diffusion limited sodium de-/intercalation process, while the sloping region (corresponding to the range of S/S' peaks in CV) is a velocity controlled adsorption/desorption process occurring at well accessible surface-sites. According to the GITT titration, the average transport speed in the slope region is higher than in the plateau region in both charging and discharging processes, as typical to a fast-capacitive behavior compared to the relatively slow Na (0) intercalation. The "adsorption–intercalation" mechanism can therefore be considered as schematically illustrated in Figure 5c as closer to the reality. The charge storage capacities contributed from the slope and plateau regions at different cycles were also calculated and are plotted (Figure 5d,e). It was found that the capacity fading of the hard carbon anodes is mainly due to a fast decay of the plateau capacity, while the supercapacitive slope region is significantly more stable. Therefore, it is further deduced that the gradual damage of the graphitic nanodomains in the hard carbon due to intercalation expansion is a main reason for the irreversible capacity loss.

Although the "adsorption–intercalation" mechanism is well-supported by a larger number of recent studies, a more general thermodynamic description of this behavior would still simplify the discussion. Indeed, contradictory or new models continue emerging to add the obviously missing facets.[29,78–80] There are, for instance, remaining concerns on the sequence of Na ion adsorption and intercalation, whether the two processes are separated or concurrent in the intermediate state. In addition, profound understanding of the local interaction between the sodium and the respective adsorption sites is missing, that is,

a simple view on carbon (beyond electrochemistry) as an electronic and thereby active sorption material is eagerly requested. For example, heteroatom doping (especially nitrogen) into carbon materials has been widely considered as an effective method to enhance the sodium storage performance by increasing the electrical conductivity, providing abundant localization sites, and in some cases, expanding the interlayer spacing for better transport.[32,81,82] Considering the structural complexity of carbon materials derived from the various precursors, it is a challenging task to isolate the relative contributions of single factors as all structural features are more or less related with each other. Therefore, a holistic view on sodium storage mechanisms is potentially helpful.

3. Translating Electrochemical Curves into Quantitative Adsorption Isotherms

The free energy of a redox reaction, but also other energies related to a charge flow or the change of a local electric field, can be directly translated into a voltage signal based on the Nernst equation. According to Nernst, a voltage change of 1 V in a chemical reaction can be roughly translated to an enthalpy value of ≈100 kJ mol^{-1} (more precisely 96 485 J mol^{-1}) for a one electron reaction. This can be used as a "Rosetta Stone" to communicate between the world of electrochemistry and voltages and the world of thermodynamics with its adsorption enthalpies. For example, the enthalpy of the oxidation of lithium metal to Li$^+$ (Li$^+$ + e$^-$ → Li) is −299 kJ mol^{-1}, while its standard electrode potential is −3.1 V (vs SHE). The power of this transcript kicks in when we consider secondary thermodynamic
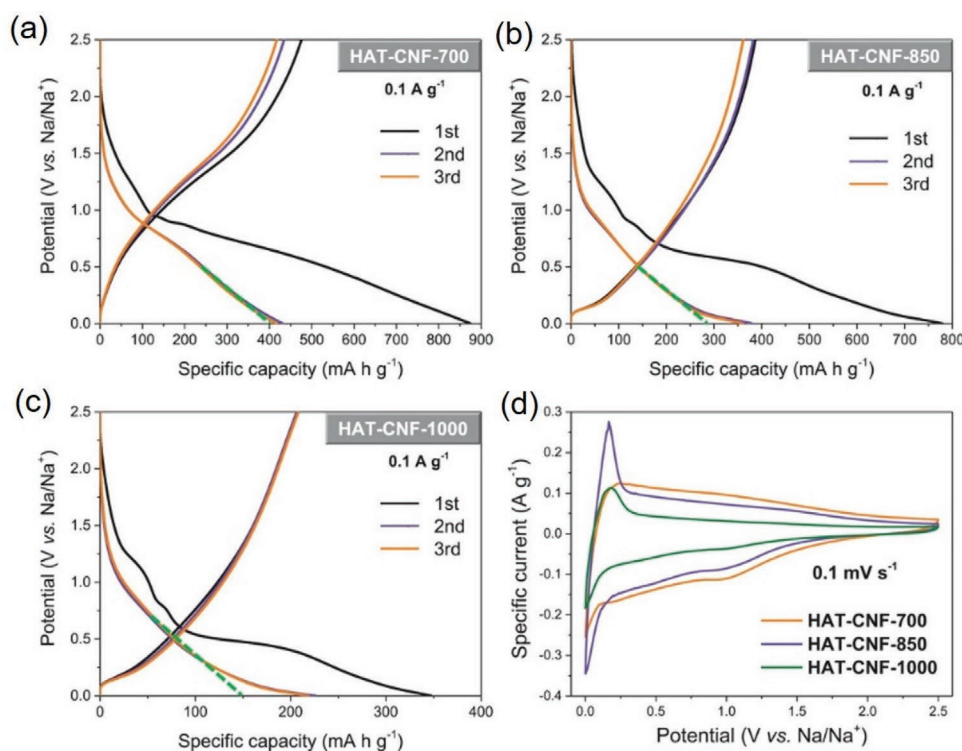
Figure 6. Anode sodium-storage half-cell tests of HAT-CNFs. Galvanostatic charge–discharge profiles of the first cycles of a) HAT-CNF-700, b) HAT-CNF-850, and c) HAT-CNF-1000. d) CV curves of HAT-CNFs scanned at a rate of 0.1 mV s^{-1}. Reproduced with permission.[84] Copyright 2019, Wiley-VCH.

processes. Throughout reduction, the Li$^+$ must be desolvated (i.e., the secondary bonds between the cation and the solvent lone pairs have to break up, and the as-generated Li(0) will readsorb onto a new place, say on its binding site between the graphene sheets (without solvent molecules, thus the two graphene layers "replace" the solvent)). All that must change the voltage, as we cannot break the law of energy conservation. Lucky enough and decisive for the choice of the electrode material, the binding of Li(0) within graphite is stronger than the binding of Li$^+$ to usually four solvent molecules. This is why a Li-graphite battery shows a drop of 0.1–0.3 V electrode potential when compared to the Li standard potential, while graphene loading in defined steps directly relates to the energetics of the different Li/C intercalation compounds.[83] (This is strictly true for reversible curves. If there is a difference between loading and deloading, this relates to dissipation and heat which is not entering ideal Nernst equation and must be considered differently).

Along a similar line of arguments, sloping curves have a very rich density of information about the adsorption sites in the material, which to our understanding in literally thousands of papers is currently not used at all. The voltage-specific capacity curves during the discharging–charging process can be translated into enthalpy-adsorbed amount curves, which can provide new aspects regarding the chemical interaction between the Na ions and electrode materials.

We will illustrate this concept along a typical literature case. Recently, Yan et al. synthesized microporous nitrogen-doped carbon fibers (HAT-CNFs) with different nitrogen contents (15, 10, and 5 wt%) as a series of model materials to investigate the contribution of sodium storage by intercalation and revers-

ible ion binding on nitrogen sites.[84] The materials were fabricated through thermal condensation of an electrospun mixture of hexaazatriphenylene–hexacarbonitrile (HAT-CN) and polyvinylpyrrolidone (PVP) at different temperatures (700 °C, 850 °C, and 1000 °C). and the products were denoted as HAT-CNT-700, HAT-CNT-850, and HAT-CNT-1000, respectively. **Figure 6**a–c shows their voltage–capacity profiles at a low current density of 0.1 A g^{-1} with the potential range of 0–2.5 V versus Na$^+$/Na during the first three cycles. It was noticed that the first loading curve presenting the initial loading process is not really a line, but has a "belly", which can be related to the chemical reactions between the electrolyte and electrode materials. This phenomenon is also observed for other carbon materials during the initial loading process.[85,86] For the following discharging from the second cycle, the "belly" will vanish, and the curve becomes smooth. All three samples showed a capacity decay from the discharging to charging process in the initial cycle, and the irreversible process is typically ascribed to the formation of a solid-electrolyte interphase (SEI) and a possible related loss of sodium to be integrated into the electrode structure. From the curves, we can see that the SEI layer essentially forms (proportional to the flown charge) at reductive potentials of –1.5 V and higher (more negative), that is, this fits with a reaction where the electrons are consumed by the reductive opening of the cyclic carbonate solvent molecules into a Na-carboxylate SEI along the carbon fibers (Step a of the revised model, **Figure 7**). This potential goes well with the known reactivities of ester reduction in organic chemistry, and it must be noted that for every transferred and thereby "lost" electron, a negative charge must stay at the SEI, coulomb-balanced by a Na$^+$. From the
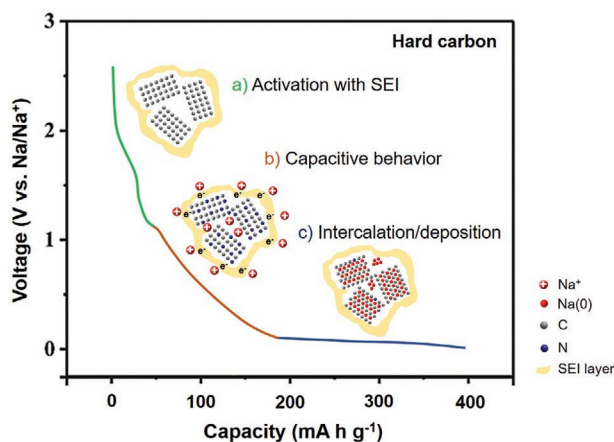
2102489 (6 of 17)

Figure 7. Schematic illustration of the revised model for sodium behavior in hard carbon during initial loading process. a) Activation under the formation of SEI layer. The resulting jelly hybrid material acts as the host material in further cycles instead of initial pure hard carbon, which alters the sodium adsorption significantly. b) Capacitive storage of sodium ions in the hybrid material, to be divided into the capacitive storage in the SEI layer and along the carbon material. c) Metallic sodium intercalation along the graphene layer and deposition in pores.

difference in charge of the first loading and deloading cycle, we can then directly calculate the molar amount of SEI, and we come up with one created negative charge and lost sodium per about 70 mass units of the former carbonaceous electrode. This means that the weight of the SEI is in the specific, discussed case, bigger than the weight of the former carbon. Clearly, after the first loading/deloading, the carbon electrode is not a pure carbon structure anymore, but half-filled with an ionomer presumably being not only around, but also inside the carbon. The interpretation of further loading and deloading curves has to be seen under this restriction: it is not a hard carbon being cycled, but rather a jelly hybrid material. Further sodium uptake is, of course, massively altered by the apparent omnipresence of SEI ion pairs in the system and the creation of a polar, ionic environment.

In the following cycles, all carbons, but especially those condensed at 850 °C and 1000 °C, show a double sloping where most of the energy is re-found in a triangular area, topped by a very short and steep sloping region at 1.2–2.5 V against Na^+/Na. This steep slope, as judged both by the low reductive voltage and low capacity, can be presumably attributed to the reversible binding of Na^+/electron pairs in the organic SEI. This assignment is also strongly supported by in situ impedance spectra which in this region of storage only shows a change of the SEI-related signals.[87]

The second slope with triangular shape between 1.2 and 0.3 V is well-known from supercapacitors and comes from the fact that the transferred electrons are obviously conjugated and interact within the electrode material with each other, that is, the more electrons you want to put in, the higher the voltage must be. The storage capacity of this mode (the intercept of the green dashed line with the capacity axis) showed a linear relationship with the nitrogen content (420, 298, and 146 mAh g^{-1} for the 15, 10, and 5 wt% nitrogen content, respectively). Therefore, the capacity of this region can be assigned to the reversible binding of sodium ions onto the nitrogen-containing

sites of the porous and defect-rich HAT-CNF surface. Interestingly, this mode is not active from zero voltage, but needs ≈ -1.8 V reductive potential from the start, that is Na^+ can only bind at a nitrogen site with highly negative bias potential; the original N-carbon is not able to bind Na^+ from solution. This is also wrongly described in many previous papers where the authors obviously do not consider the thermodynamics of adsorption processes. In the language of adsorption, these sites come therefore with an energy loss of ≈ 180 KJ mol^{-1} to bind a sodium, which is presumably related to the partial desolvation of the Na^+, well-predicted to be exactly in this region. The -1.8 to -3.0 V electrons are counter-localized within the (now highly conductive) carbon framework, as seen by the supercapacitor-like loading behavior.

The loading capacity contributed by this region can be easily translated into the amount of sodium stored. For example, a capacity of 420 mAh g^{-1} for HAT-CNF-700 represents a sodium capacity of 15.7 mmol$_{Na}$ g^{-1}, which means that one nitrogen atom in HAT-CNF-700 relates to 1.5 sodium atoms. Similarly, these values were calculated for HAT-CNF-850 and HAT-CNF-1000 and were found to be close to 1.5 as well. Therefore, we can state that the sodium storage in this triangular sloping region can be related to the nitrogen functional groups, but it is more an indirect influence of nitrogen on the electronic structure and the accessible specific surface area rather than site specific binding as we can "overbind" Na^+ by 50 mol% (Step b of the revised model, Figure 7). Similar trends were also reported by other groups. For example, Au et.al also demonstrated that each defect in the oxygen-containing hard carbon corresponded to more than one sodium through comparing the theoretical capacity and experimental data, which is in good agreement with our results.[88] Their DFT simulation further supported that the effect of defects in carbon structures was delocalized and they influenced the sodium behavior at the defect site as well as the sites near the defects.

This supercapacitive energy storage is terminated by a maximal voltage, when the reduction potential of Na^+ is reached. Then, it becomes energetically more favorable for the system to reduce the Na-ions, or in other words: the electrons at these high negative voltages move from to carbon to the Na^+ for reduction, and Na (0) is formed, which then integrates into the anode material as a different species.

For this-potential region below 0.3 V versus Na^+/Na (Figure 6a–c), HAT-CNT-700 has only minor capacity, as no additional Na^0 binding sites, while both the HAT-CNT-850 and HAT-CNT-1000 start to show a short plateau (Step c of the revised model, Figure 7). This phenomenon is in good agreement with the increased degree of graphitization and expanded interlayer spacing when the HAT materials are subjected to higher pyrolysis temperatures, and this promotes the possibility of additional Na(0) intercalation in the graphene stacks. The plateaus can also be measured as a peak of 0.2 V in the CVs (Figure 6d) of the HAT-CNF-850 and −1000, while the rest of the CVs are capacitive-like, all that further confirming our assignments and interpretations. A similar phenomenon was also reported by others. For example, a series of carbon materials was prepared by direct pyrolysis of ginkgo leaves at 600–2500 °C. The carbon sample obtained at the lowest temperature of 600 °C also showed only a sloping region without any plateau region in the charge/discharge profiles. Accordingly, it showed wide humps without obvious sharp
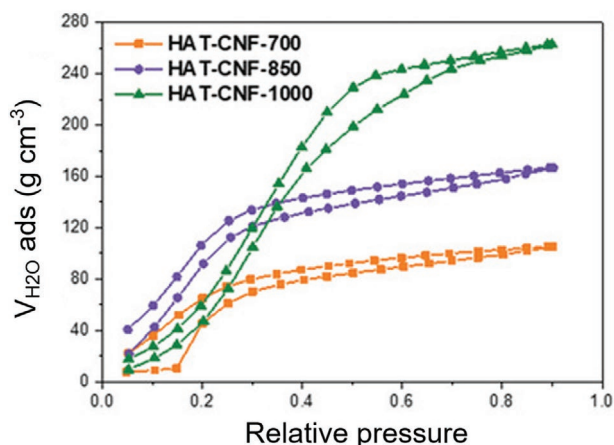
Figure 8. Water vapor physisorption isotherms (at 25 °C) of HAT-CNFs. Reproduced with permission.[84] Copyright 2019, Wiley-VCH.

peaks at low potential, underlining capacitive behavior. In contrast, the other carbon samples prepared at higher temperature showed sharp peaks at ≈0.1 V, corresponding to their intercalation/deposition behavior.[89] The formation of Na(0) or Na clusters than their ionic form were also verified by in situ NMR and ex situ X-ray photoelectron spectroscopy (XPS) in both low and high-temperature-treated carbon.[90,88,46]

To receive further information on the strength of interaction between the HAT-CNF samples with sodium species, Yan et al. also conducted water vapor adsorption at 25 °C at exactly the same materials and used the water molecule as a representative of polar species, however, being free of electron-electron repulsion. As shown in **Figure 8**, HAT-CNF-700 and HAT-CNF-850 show higher adsorption at relatively low pressure below 0.2, while HAT-CNF-1000 shows much higher binding overall, however, at a relatively high pressure. The low-pressure step reflects a higher enthalpy of water adsorption on the carbon materials with higher nitrogen content, indicative of a stronger interaction between water and HAT-CNF-700 than HAT-CNF-850 and HAT-CNF-1000. This effect has been reported also in the field of gas adsorption; carbon materials with high content of heteroatoms, exhibit partly very high adsorption enthalpies to molecules (e.g., CO_2).[91,92]

The step height in the sorption isotherm corresponds to molar amounts. In these experiments, the water bound to the surface in strong adsorption mode is 4.4 resp. 7 mmol g^{-1} for HAT-CNF-700 than HAT-CNF-850, and we tend to attribute those sites to the capacitive Na^+-binding sites. It is, however, exciting to see that the materials can obviously bind more Na^+ than H_2O, that is, either the Na^+ taken up in the anode is not solvated, or the jelly SEI structure also within the material plays an amplifying role changing the dispersion of the carbon and making more binding sites accessible. HAT-CNF-1000 with its lower nitrogen content and much higher degree of graphitization binds much higher amounts of water more weakly, and there is no correlation between low energy water binding and Na-binding is lost, that is those sites are not relevant for battery processes.

The strong interaction of polar adsorbates with N-doped carbon is by computer models, attributed to the high polarity of nitrogen-doped carbon materials induced by the positively

polarized carbon atoms and negatively polarized nitrogen atoms. A potential adsorption enthalpy value of sodium species of 100 kJ mol^{-1} on a −2.7 V electrode (the transition point from Na^+ to Na^0 deposition is close to the heat of evaporation of metallic sodium (97 kJ mol^{-1}). This opens up the possibility that the deposited sodium is not necessarily metallic or plated as a film (sometimes leading to dendrites), but can be also in the form of neutral atoms or small clusters, as sodium at such surfaces is then isoenergetic with bulk sodium. It has already been reported that the increased binding to nitrogen-doped carbon materials compared to unmodified carbon is beneficial for relieving the formation of sodium dendrites, and the assumption is nearby that this is directly related to the strong support interactions as quantified above.[93–96]

An interesting additional thought can be extracted from recently described supercapacitor experiments. Here, a series of porous carbon nanomaterials were analyzed as electrode materials of supercapacitors in 1-ethyl-3-methylimidazolium tetrafluoroborate (EMImBF$_4$) as a model ionic liquid (IL) and cycled between 0 and 3.5 V, that is, in the same voltage range.[97,98] Considering the behavior of Na ions involved in SIBs anodes within the slope region to be capacitive, the analysis in this study could also be helpful to contribute to the binding mechanisms in SIB anodes.

When the micropore size of the carbons matched that of IL ions (marked as STC-16), an asymmetric triangle of the galvanostatic charging/discharging curves at a low specific current density of 0.5 A g^{-1} (**Figure 9**a) was found, and most of the storage was indeed typical double-layer capacitor behavior.[97] However, a pair of reversible peaks at ≈0.6 V was observed in the CV curves of STC-16 with matched micropore size (Figure 9b), together with an emerging peak at higher cell voltages. Interestingly, the peak at 0.6 V disappeared again for the sample where STC-16 was additionally CO$_2$-etched (marked as Ac-STC-16), which had an almost preserved structure but a higher surface area than that of STC-16 and thereby not ion fitting pores. The possibility of redox reactions for this peak was ruled out in terms of their rate-dependent performance.

As discussed, a voltage of 0.6 V for this transition can be translated into an enthalpy of ≈60 kJ mol^{-1}, and it was reasoned that this peak likely originates from the insertion of single ILs ions into the micropores. That means a single ion loses all its neighboring counterions during the insertion into the micropores, while a majority of this desolvation energy is returned from the interaction of the single ion with the oppositely charged carbon walls. The overall balance of this reaction was found to be slightly endergonic still, but again, as in the SIB anodes described above, this can be compensated by the 0.6 V bias potential, that is, electricity activates otherwise non accessible adsorption processes and stores energy as such. With the potentially much stronger interacting Na, such transitions might indeed occur throughout the loading for Na^+/electron "adsorption" pairs, then at higher potentials. Also, the transition between single atom Na(0) and metallic Na is expected to be moderated by micropore size, and to control the right size of Na-clusters by pores might turn into a safety relevant issue for the suppression of dendrites.

For Na batteries, there is a potentially most relevant final 4. mode of energy storage, which is the deposition of metallic
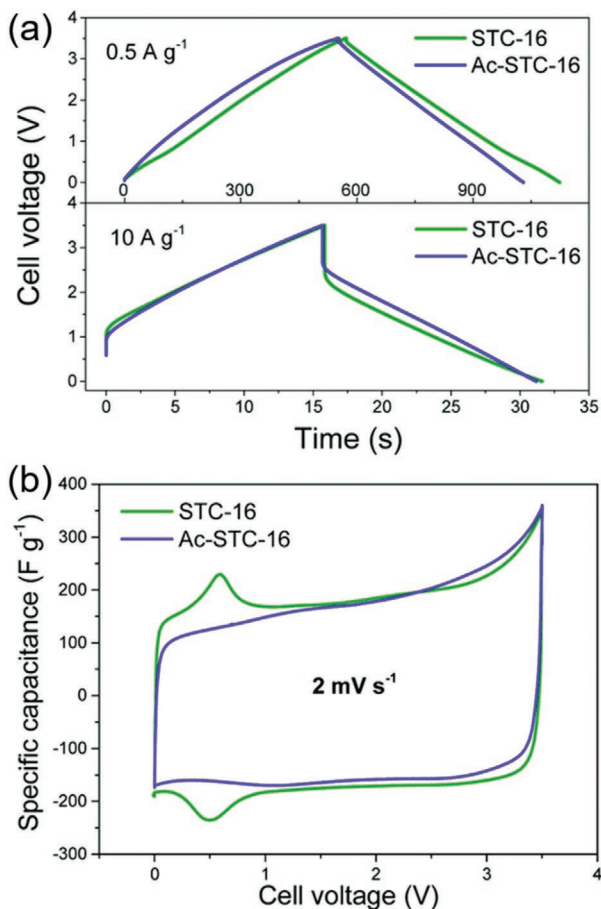
ADVANCED
SCIENCE NEWS
www.advancedsciencenews.com

ADVANCED
ENERGY
MATERIALS
www.advenergymat.de

Figure 9. Electrochemical performance comparison of STC-16 and Ac-STC-16 tested in EMImBF$_4$ ionic liquid using a two-electrode configuration: a) charge/discharge profiles at different specific currents. b) cyclic voltammograms at a scan rate of 2 mV s^{-1}. Reproduced with permission.[97] Copyright 2018, Wiley-VCH.

By the rules of thermodynamics, a peak overpotential is required for Na nucleation during the loading process, as it involves a first order phase transition. This however can also be modified by surface effects. Recently, plating-like Na-deposition was surprisingly also observed to start well below the standard reduction potential of Na, and continued to occur there for a rather high charge capacity. In this work, Chen et al. prepared an ultrathin carbon nitride (g-C$_3$N$_4$) film deposited on a classical, dense, and flat copper metal electrode via chemical-vapor deposition.[101] When employed as anode materials for SIBs, a highly reversible apparent capacity of up to 51 Ah g^{-1} C$_3$N$_4$ was achieved. This value beyond the theoretical limit points to a wrong weight division by the expected "electrode material" and indicates that Na deposition does not occur in the g-C$_3$N$_4$, but mostly as underpotential plating below the carbon nitride. Previous studies had shown that the thin g-C$_3$N$_4$ with its highly polar organized pores is permeable for Na ions as well as it has good electrolyte wettability. Therefore, it is reasonable to assume that g-C$_3$N$_4$ works as a SEI layer for Na ion transport. A model (**Figure 10**) was built further to reveal the rationale behind this phenomenon. Due to the high HOMO position or work function of carbon nitride ($\approx$ +1.5 V) compared to that of Cu (+0.34 V), spontaneous charge transfer from Cu to carbon nitride will occur, and a Schottky layer will form, thus a local potential shift of up to 1.2 V as compared to outside electrodes can be expected (Figure 10a). This is nicely consistent with the experimentally determined underpotential of 1.2 V for Na(0) deposition. Na(0) can obviously form at lower outer voltages, as the missing energy can be locally added by the back transfer of electrons to the Schottky zone of the copper (Figure 10b). It is understandable that with the increasing thickness of sodium layer, the electron back donation becomes less and less relevant, and the underpotential finally vanishes at a maximum thickness of 500 nm (Figure 10c). As driven by this very local mechanism, Na (0) is therefore deposited in a controllable way only near the heterojunction zone, while of course, dendrite formation or uncontrolled Na deposition is still thermodynamically forbidden. This model of underpotential Na deposition points a way to new "nanoplating"-designs, as similar electron poor zones can be realized in other packed 1d- and 2d hybrid materials.

4. Resulting Effective Strategies Toward Better Performing Carbonaceous Materials for Future Anodes of SIBs

As described above, there are along the presented model, at least no less than three different, consecutive modes of energy storage in Na anodes. The initial process related to the activation of SEI can be improved by reducing the surface area or optimizing the electrolyte. The following three steps can be independently optimized by materials design (**Figure 11**): a) capacitive storage, potentially splitting up in capacitive storage in the SEI, and capacitive storage in the carbon material (potential of 1.2–0.3 V); b) underpotential sodium deposition and intercalation (potential of 0.3–0 V); and c) overpotential, nucleated sodium plating (slightly positive potential). These three modes will be discussed in the sequence of their occurrence in the loading cycle, that is, from low voltages to high voltages.

sodium on the surface of the anode. This "metal-plating" occurs in principle on the surface of every conductive material at overpotential conditions and is considered "unsafe", as it usually leads to kinetic and electric field enhancements at tips to end up in dendrites. That can (i) constantly break and re-form the SEI and thus cause poor cycling stability, (ii) puncture the separator, (iii) result in detachment of dendrites and formation of "dead Na", and finally (iv) cause connection of the electrodes and partly violent shortcut of the battery.[99,100] In principle however, this mode enables to approach the theoretical maximal capacity of metallic Na (1166 mAh g^{-1}), and it is the art of materials design in it to avoid dendrite formation by physical means, that is, special thermodynamic and kinetic conditions to be established by chemical interaction.

Metal plating usually occurs in "overpotential mode", that is, at more negative potentials than the standard potential. Several steps are involved in the electroplating process, including the ion transfer from the electrolyte, charge transfer, atomic surface adsorption, surface diffusion, sodium nucleation, and final growth, and all that can be controlled by the chemistry of the electrode materials.

ADVANCED
SCIENCE NEWS
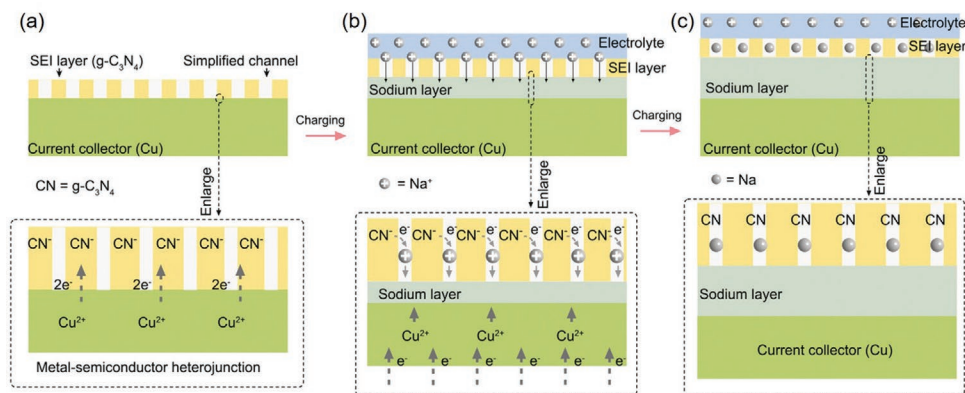www.advancedsciencenews.com

ADVANCED
ENERGY
MATERIALS
www.advenergymat.de

Figure 10. Illustration of the mechanism of the sodium storage in the Schottky layer of a g-C$_3$N$_4$ film activated Cu foil. a) The g-C$_3$N$_4$ deposited on Cu foil (current collector) constitutes a metal–semiconductor heterojunction in which electrons will transfer from copper to g-C$_3$N$_4$, creating an electron poor zone. b) In the charging process, Na ions permeate through thin g-C$_3$N$_4$ films and are reduced onto the Cu metal at underpotentials, thus forming a Na compound layer. The energy related to underpotential corresponds to the change of the work function in the Cu surface, thus stabilizing metallic sodium in an electronically changed interface state. c) The state after charging: sodium metal acts as the anode material and the g-C$_3$N$_4$ film works as SEI to avoid direct contact of the metallic sodium and liquid electrolyte. Reproduced with permission.[101] Copyright 2020, Wiley-VCH.

First and in many cases even the strongest contribution, sodium storage in carbonaceous materials mainly relates to the capacitive Na$^+$ adsorption on surface sites, while the previously loaded electron is delocalized into the SEI and/or conductive electrode materials. Accordingly, an increase of accessible active sites (e.g., defects, pores, or specific surface area) for adsorption/desorption is effective to boost the sodium storage performance. Up to now, some effective strategies including heteroatom doping, porosity engineering, and electrolyte optimization have been broadly studied, as discussed below.

Second, the underpotential plateau deposition is probably related to Na(0) intercalation between graphitic sheets or in so called slit-pores, which is thermodynamically only possible for stacked carbon structures expanded in comparison to pure

graphite. This mode seems to be (as it is well-known from the Li-battery) the first to think about, but is the most difficult to optimize, as on the one hand, less Na than Li can be intercalated, for size reasons, as well as this mode comes with expansion stress onto the stacks, and thereby rather quickly destroys current electrode materials.

Third, overpotential Na plating seems to prefer mesopores and interstitial cavities inside tectonic electrodes, while on the surface of such structures, wetting and sodium nucleation must occur. This can be supported in the material by polar, heteroatom modified, or coated carbon surfaces.

In this tutorial review, we mainly discuss for these three processes, the chemical strategies of heteroatom doping, interlayer expansion, and surface modification, as well as different pore structures.
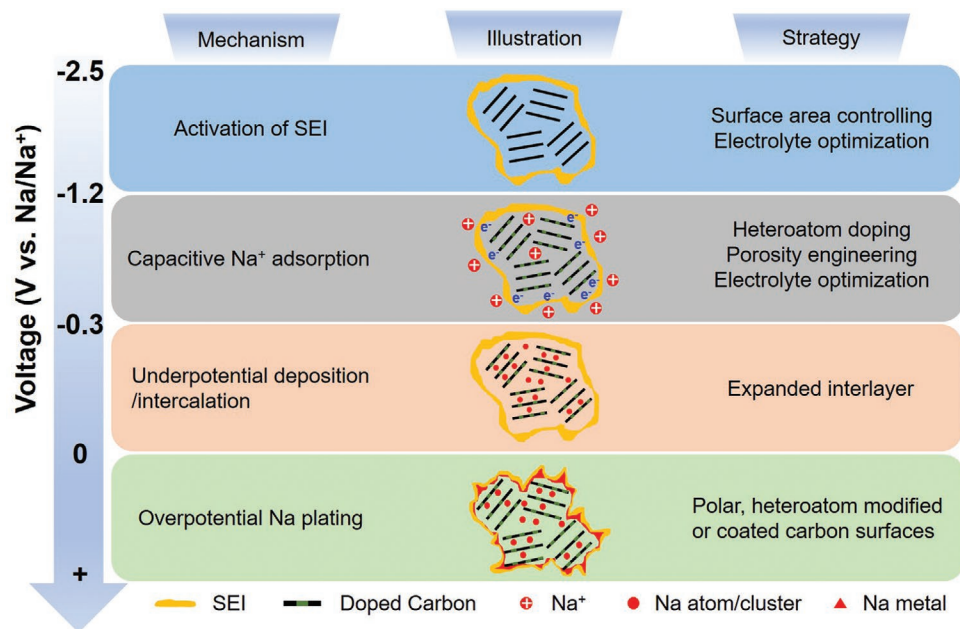

Figure 11. Illustration of the mechanism at different potential range and corresponding strategies.

2102489 (10 of 17)

**ADVANCED
SCIENCE NEWS**
www.advancedsciencenews.com

**ADVANCED
ENERGY
MATERIALS**
www.advenergymat.de

4.1. Heteroatom Doping

Heteroatom doping in carbon materials refers to guest atoms covalently substituting the carbon atoms in typical carbon structures, for instance in the graphitic planes and edges. Among many options, four heteroatoms are most regularly used, which include nitrogen (N), boron (B), sulfur (S), and phosphorus (P). The doping of a conjugated structure with those heteroatoms tends to induce structural defects as well as changed electronic states in the carbon materials, which provides the adsorption sites and/or reaction sites for reversible Na^+ binding.

There are extensive reviews available on heteroatom doping so we only point to aspects related to SIBs.[102] To summarize the key features of previous reviews: there are clear structural influences of the heteroatoms (**Figure 12**), such as that S is much bigger than carbon, will disturb graphitic packing, and will be placed on at edges and within five rings. Neither B nor N as such do well within graphitic planes, and most of them are found by XPS in edge connection motifs, which in the present context means a missing covalent bond per heteroatom, potential surfaces and pores, and thereby a potential Na^+ binding site. As a second contributor, mostly ignored by simplified local models, heteroatoms come with a different electroaffinity and change the work function, that is, the redox potential change of the electron pool of such doped carbon is partly massive.[103]

Nitrogen doping is most advanced in the literature to enhance the sodium storage properties of carbon-based electrode materials. The nitrogen sites donate free electrons to the
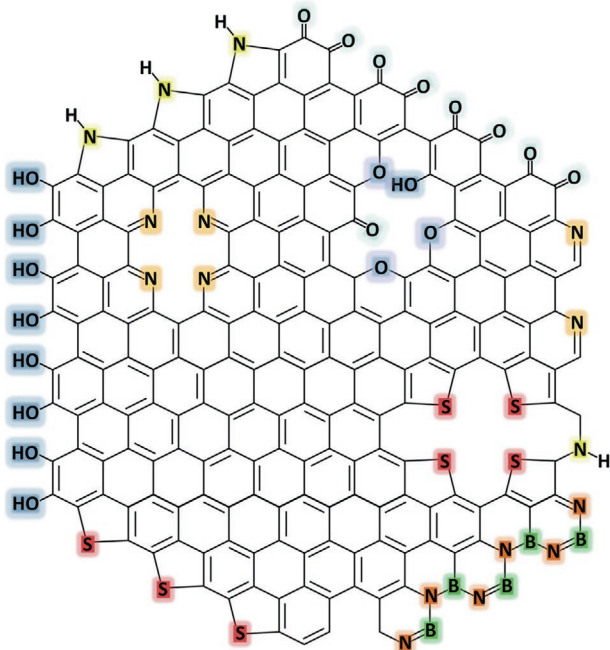
conjugated carbon, resulting in increased electrical conductivity and thus improved charge-transfer and ion transport processes. For example, a nitrogen-doped carbon nanotube film was reported with an electrical conductivity of 410 S cm^{-1}, which is twice as much as the pristine CNT film.[104] N as described, adds surface area, pores, and direct adsorption sites for Na^+ and thus an increased slope capacity which at the same time, as capacity, is usually long-term stable. N and S modification also contribute synergistically to the other sodium storage modes. For example, the doping of S into N-rich carbon nanosheets does not only provide more adsorption sites and surface area but also enlarges the interlayer stacking distance, both of which gives rise to high capacity and excellent rate performance of SIB anodes.[105,106]

Recently, Jin et al. reported the successful synthesis of N, B co-doping 2D carbon nanosheets (NBTs) using H_3BO_3 as templates and low-cost gelatine as carbon precursors (**Figure 13**a).[31] The 2D nanosheet structure and heteroatom doping was shown to be beneficial to improve the electrode/electrolyte contact, created defects, and active sites for Na^+ adsorption and thus achieved improved storage capacity (309 mAh g^{-1} at 0.2 A g^{-1} for 200 cycles), excellent rate performance (192 mAh g^{-1} at 10 A g^{-1}), and an already acceptable cyclability (225 mAh g^{-1} for 200 cycles at 1 A g^{-1}). The sodium storage mechanism was also studied using ex situ X-ray diffraction (XRD) measurements at different states during first charge/discharge process. It was found that the (002) peak was unchanged during the discharging process from 2.6 to 0.2 V, while it shifted to low angle after being discharged to 0.01 V, which is in agreement with the "adsorption–insertion" storage mechanism presented above. The CV measurements at different rates (Figure 13b,c) confirmed the predominantly capacitive storage mode in these N, B co-doped 2D carbon nanosheets (95.0%, 95.6%, 96.9%, 97.1%, 99.2%, and 99.4% at scan rates of 0.1, 0.3, 0.5, 0.7, 0.9, and 1 mV s^{-1}, respectively) compared to those of the all carbon references (56.9%, 64.7%, 71.2%, 75%, 80.5%, and 84.1% at corresponding scan rates). This illustrates the role of N, B co-doping for promoting essentially the capacitive storage of Na^+. A high-proportion of slope capacity and thereby, supercapacitor-like behavior usually comes with excellent rate performances and cyclability, and it was also found in these examinations. In addition, theoretical calculations were added to support that the pseudocapacitive-dominated Na^+ storage process takes profit of the increased electronic conductivity and promotion of Na^+ adsorption.

Although heteroatom doping has been largely reported as an effective method to enhance the Na^+ uptake, the presence of edges and excess surface area brought by the heteroatom doping promote excessive SEI formation when inappropriate chemistry is applied, as discussed above. To deal with this problem, Alvin et al. prepared P-doped hard carbon by simply mixing lignin with phosphate, filtering the mixture to remove unabsorbed PO_4^{3-}, and carbonized the material at a high temperature of 1300 °C.[107] Through controlling the heteroatom doping at a low level of 1.1 at%, SEI formation could be reduced to 28% of the primary charging capacity. We take this as an indication that with heteroatom-doped carbons, SEI design has to be more advanced (than only trusting in a favorable side reaction) to balance the storage capacity, cycling stability, and SEI losses in the first charging.

Figure 12. Illustration of how heteroatoms create missing covalent bonds. Any heteroatom doping reduces covalent connectivity and comes thereby in groups and patterns (due to the rules of graphene geometry and covalent bonding). Graphite has three covalent neighbors, while heteroatom defects usually come with two. This change automatically brings surface area, porosity, and defect binding sites, but also lowers material density and higher polarizability. Higher order effects of heteroatoms as curvature, undulations, or thickness variations are for simplicity not presented.

ADVANCED
SCIENCE NEWS

www.advancedsciencenews.com

ADVANCED
ENERGY
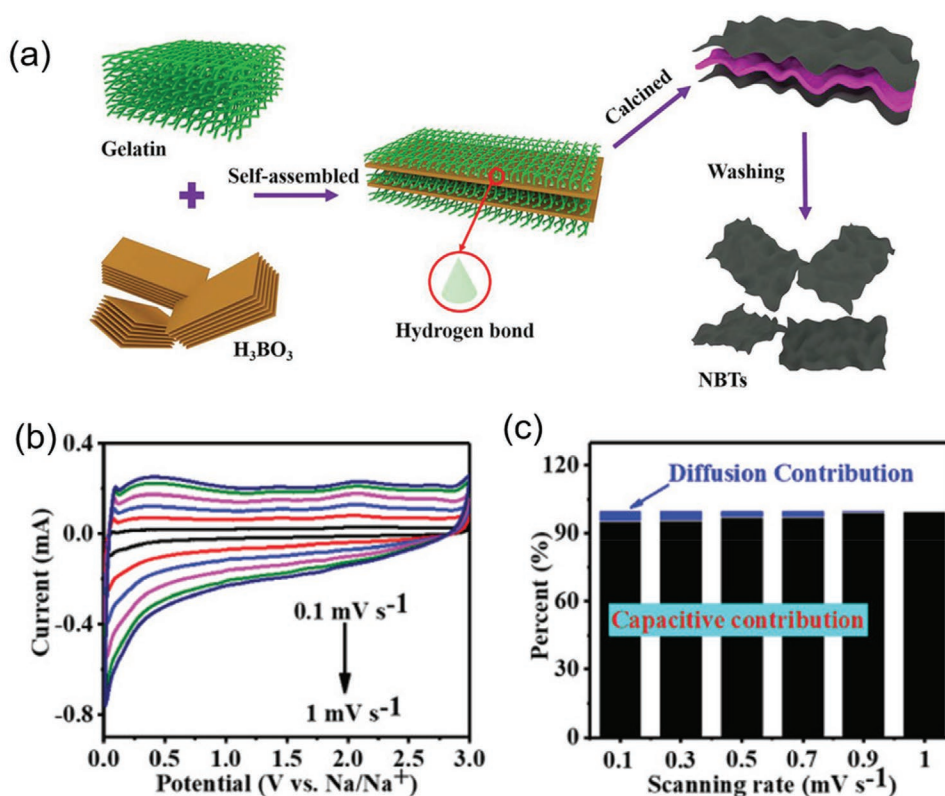**MATERIALS**

www.advenergymat.de

Figure 13. a) Schematic illustration of N, B co-doping 2D carbon nanosheets (NBTs) using a template assisted method. b) The CVs for NBT700 at scan rates of 0.1–1 mV s^{-1}. c) The capacitive and diffusion contribution ratios for NBT700 at different scan rates. Reproduced with permission.[31] Copyright 2020, Wiley-VCH.

4.2. Expanded Graphene Interlayers

It was already mentioned that the larger radius of Na$^+$ (1.02 Å) compared to Li$^+$ (0.76 Å) hinders direct graphite intercalation: graphite as the commercial anode of LIBs is electrochemically inactive in SIBs. Distortion of in-plane structure and thereby packing, increases interlayer spacing of carbonaceous materials and opens the way for sodium intercalation. Previous studies indicated that the Na$^+$ can undergo insertion/extraction when the graphene layer spacing exceeds 0.37 nm. For hard carbons, a d spacing within the general range of 0.37–0.4 nm is thereby suitable for Na intercalation, and it varies with the types of precursors and post-treatment procedures. The problem of this mode of sodium storage is the huge structural strain through loading/deloading bringing the mechanical disintegration of the materials structure and rapid capacity decay, a problem to be alleviated by structural design.

Hu et al. prepared a hard carbon-based anode material with expanded interlayer spacing through mixing the as-obtained N-rich hard carbon with a NaCl aqueous solution, followed by hydrothermal treatment.[108] During the hydrothermal reaction, the salt could intercalate into the hard carbon and enlarged the interlayer distance, evidenced by high-resolution transmission electron microscopy and increased specific surface areas. Compared to the samples without treatment, a 100% improvement of specific capacity was achieved after NaCl intercalation. Pillaring modified graphenes by inclusion of inert inorganic

salts and clusters might thereby be a promising experimental approach.

Up to date, some of the alkali metals including K and Ca ions were doped into the hard carbons and their enhanced performance of SIB were reported.[109,110] The benefits mainly lie in the expansion of graphene interlayer by insertion. The influence of the expanded interlayer spacing on the sodium storage was also investigated by Wu et al.[109] They used coconut shells, which are naturally rich in K$^+$, as the precursor to synthesize the carbon (**Figure 14**a). Due to the large radius of K$^+$, the K$^+$ insertion could effectively expand the interlayer spacing of hard carbon. Through varying the pyrolysis temperature from 900 to 1200 °C, the d-spacing of (002) planes ranged from 0.387 to 0.401 nm, as determined by the XRD measurements (Figure 14b). Among those samples, the hard carbon obtained at 1100 °C with the largest interlayer spacing (0.401 nm), delivered the highest charge capacity of 313.8 mAh g^{-1} with the highest ICE where "only" 31% of charge was lost for SEI formation, that is, the SEI ionogel does not form between those layers. The high capacity is in good agreement with previous studies that the insertion capacity for hard carbons in SIB anodes increases with increasing interlayer spacing up to 0.415 nm.[65] It should also be noted that the discharge and charge plateaus (Figure 14c) are slightly less negative than metallic sodium. This endows the carbon-based anode at the same time with a high ICE and good cycling stability. According to our thermodynamic reading of the voltage curves on the enthalpy scale, this
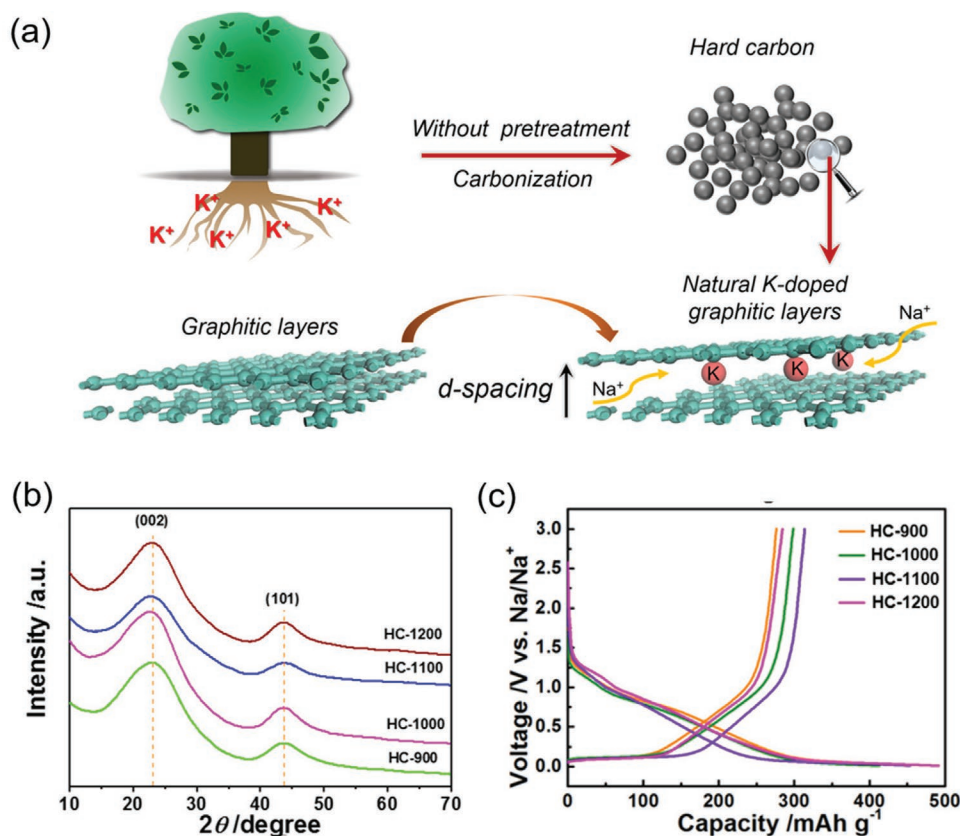
Figure 14. a) Schematic diagram of the synthetic route for natural k-doped hard carbon anode. b) XRD patterns and c) initial voltage profiles of hard carbon materials at a current density of 50 mA g^{-1}. Reproduced with permission.[18] Copyright 2015, American Chemical Society.

difference to the standard sodium potential indicates a weaker back-stabilization of Na(0) and the graphitic sheets at higher interlayer spacings. Comparing these and other data, it looks like the smaller the interlayer distance, the slower the insertion but also the better the back stabilization of the sodium atoms and the less negative the plateau voltage, with the voltage difference quantifying the Na–C interaction energy.

4.3. Overpotential Deposition, Nucleation, and Plating of Metallic Na in Pores and Interstitials of Textured Carbon Electrodes

Sodium plating likely occurs at slight overpotentials, following the interlayer intercalation in the underpotential plateau. Extensive research efforts also explored this region of energy storage and are devoted to the suppression of Na dendrite growth and promotion of uniform Na plating/stripping. This was found to be largely dependent on the surface texture of the electrodes. Up to date, those effective strategies toward suppressing the Na dendrite growth can be classified into the following approaches: (i) utilizing a conductive matrix with high surface area, (ii) improving the wettability of hosts (i.e., the affinity between the Na and host) through surface modification, and (iii) engineering the pore structures.

3D carbon hosts with a high surface area have been considered as a straightforward approach for homogenizing the

Na-ion flux. They reduce the local current density (i.e., growth rate), thus ensuring more uniform nucleation and deposition of metallic Na all over the structure. The affinity between metallic Na and specific functional electrode sites can also intrinsically determine the Na heteronucleation and growth behavior. In other words: the wettability and the adsorption enthalpy between Na metal and the host materials are the primary parameters to direct Na nucleation, at best, as already stated, with an interaction energy higher than sodium evaporation enthalpy. This is a further difference between LIBs and SIBs: lithium has a higher cohesion energy than sodium, and this is why the control of sodium deposition is in the correct energy range to be directed by chemical surface modifications.

For Na, various surface modification strategies toward the 3D host materials have been proposed to enhance the binding strength with Na metal, including introduction of functional groups,[111] regulation of defects or dopants,[112,113] and modulation of interfacial composition.[114] Conductive carbon-only frameworks possess a poor affinity to Na, and thereby Na-metal deposits mostly in high field regions on the outside and stays badly controlled. Partially reduced graphene oxide (r-GO) was employed as a wetting host for Na metal, where remaining carbonyl and alkoxy groups on the surface had strong affinity for Na and thus promoted the deposition on r-GO.[115] Worth underlining, this strategy has been demonstrated to be practicable also for potassium metal batteries.[116] A sodiophilic surface was also obtained through introducing the oxygen functional

ADVANCED
SCIENCE NEWS
www.advancedsciencenews.com

ADVANCED
ENERGY
MATERIALS
www.advenergymat.de

groups or heteroatoms onto the 3D carbon nanotube networks, which can provide homogeneous active sites and guide more uniform Na nucleation.[113]

In addition, the pore-and-wall structure of carbon formed during the pyrolysis plays a key role in promoting the SIB performance by rendering the electrolyte accessibilty and thus, fast diffusion kinetics of Na ions. The filling of pores with Na will occur once the defect sites and interlayer spaces are occupied, until the electrode is fully sodiated. In this case, the capacity is closely related to the pore volume. Au et al. reported that the material carbonized at 1500 °C possessed the highest volume of open pores and thus achieved highest capacity.[117] On the other hand, Zhang et al. reported that the Na deposition mostly takes place in "closed pores" (i.e., pores that are not seen with nitrogen sorption experiments), evidenced by the excellent electrochemical properties of hard carbon with the largest closed pore ratio.[57]

The origin of these apparently contradictory findings can be traced to our opinion about the diversity of structures of the analyzed hard carbons and a missing geometric/functional descriptor for the obviously special type of pores being relevant for sodium cluster deposition, for example, classical gas sorption experiments and the related "specific surface areas" obviously are not able to describe the features relevant for sodium cluster deposition. We are however rather sure that a proper balance between the different structural factors promotes the SIB performance also in the sodium cluster storage mode, and finding a simplified descriptor based on a non-electrochemical technique is an open quest.

5. Summary and Perspectives

The sodium ion battery is a potentially promising grid-scale energy storage technology due to the abundance of Na, low cost of fabrication, and the similarity to Li, which simplifies access to all other battery components. However, it is still essential to develop high-performance electrode materials, especially anode materials for SIBs, which is best based on a more thorough understanding of the sodium storage mechanisms.

We have reviewed here the reported progress on the sodium ion storage mechanisms in carbonaceous and hard carbon anode materials, and we discussed the assignment of the diverse storage mechanisms to the different regions of the voltage profile. Interpretations in the frame of the interaction between the sodium and electrode materials could be obtained by translating the voltage–capacity curves into enthalpy-adsorbed amount curves based on the Nernst-equation and comparing those values with otherwise reported interaction processes, as in gas sorption or solvation experiments. Like that, SEI formation was quantified from the electron losses in the first charging/discharging cycle.

Up to two types of sloping regions were related to capacitive uptake of Na^+/electrons pairs either in the SEI or at surface sites of the carbons, and the related capacity does depend on specific surface area and heteroatom content. This storage mode is terminated when the triangular loading potential cuts the reduction potential of Na^+. After this crossing, it is thermodynamically more favorable that Na^+ and the electron

recombine, and Na(0) is to be stored. This is done in a (first) plateau region where Na(0) is intercalated only into expanded graphitic stacks. From experimental reports, a stacking distance of 0.4 nm seems to be favorable, and this can be realized by functionality and structural defects in the sheets, doping with (big) heteroatoms, but interestingly also pillaring intercalations, for example, by inert salts. Classical hard carbons usually do not withstand the expansion/shrinking stress exerted through loading/deloading so that the plateau capacity is usually not durable, but we can expect supramolecular pillaring to be more reversible and even self-healing. Interestingly, the underpotential (with respect to pure metallic sodium) at which the plateau occurs depends on some chemical parameters but mostly the stacking distance, and the shorter the distance, the higher is the back stabilization of Na (0) by the carbonaceous sheets. We underline this phenomenon as it nicely illustrates how battery measurements quantify thermodynamic interactions and physical binding effects.

As a third and to our opinion, most promising mode crossing the line to the sodium metal battery is overpotential deposition of metallic sodium at distinct and controlled sites, that is, sodium plating. The usual problem of most metal batteries is dendrite formation as a kinetic phenomenon, but sodium indeed has a comparably low cohesion energy (contrary to, e.g., Li or Mg) which can be matched by Na- surface interaction energies. A number of publications already indicate that dendrite formation can indeed be tamed by control of Na-nucleation at seeds deep into texturally structured carbon architectures, for example, porous materials or fleeces. Here, battery research can take advantage of the existing knowledge in classical crystal heteronucleation and wetting effects. Also, Na will mostly nucleate from appropriate polar sites with low electronic contact resistance, while it will hardly nucleate from hydrophobic surfaces. A porous carbon grain with hydrophilic pores but a rather hydrophobic grain surface is therefore, a rather safe bet on a massive improvement.[118] Please also note that crystals usually grow at places where their overall surface energy is minimal, for example, the crossing points of fibers and other places of maximal capillarity, again a concept of colloid science useful for battery research. Another option lies in the fact that sodium deposition from sodium ions is kinetically controlled by local electric field effects, and we can enlarge the electric field either by nanostructure ("tips", "crossings"), or by chemical heterogeneity, here exemplified within the direct transition zone of heterojunctions.

All these options make us rather positive that a physicochemically "boxed in" Na-metal battery mode is a part of a future high energy, high power, sustainable, and durable Na-based storage system. As it became clear through this article, it will, however, integrate capacitive storage, intercalation storage, and well, a metal plating in one and the same carbon material, with structural complexity, most probably derived from diverse precursors. Meanwhile, the development of advanced characterization techniques combined with theoretical simulations is also of great importance for revealing the detailed structure and mechanisms.

Low ICE, which reflects the excessive formation of SEI-layers or even complete ionogels, is another challenge of current Na-batteries, and most of the literature that reported experimental Na-anode materials are indeed in reality com-

posed about half of a "SEI-structure", that is potentially located throughout the material. Novel analytic methods coupled with in situ characterization could be useful to reveal the distribution and remainder of sodium experimentally. We also have to consider "chemo-synthetic" SEIs to replace the current "fortunate side-reaction" structures, that are inert porous coating structures to avoid the contact of reduced Na-species with the solvent, which can at least minimize the ICE within battery operation. Such coatings must be ion-, but not solvent-permeable and should have sufficiently high electronic resistance, for example, come from the class of typical membrane materials.

Another path-breaking innovation can be the development of new covalent host systems related to graphic carbon, but not being carbon. For example, inspired by the high-performance N-doped carbon materials for SIBs, carbon nitrides, especially the less studied members with small band gaps (C_2N_2, C_2N, C_3N ...) are promising candidates.[101,119] This class of carbon-based materials possesses higher percentage of N heteroatoms, which are inherently tunably porous, show high electronic conductivity, and provide rich structural features to target the optimized electrochemical performance. The strong polarization on the pore walls of such carbon nitrides and pore structures in the quantum dot size also reduces the melting point of sodium, as reported by our recent studies,[120] and thus enables a liquid electron storage metal. C_3N_4 was already analyzed in battery application but rather seems to be an interesting SEI replacement material that creates strong heterojunction effects for the safe electroplating of sodium.

As a comment on the development of innovation processes, sodium in battery was previously mostly seen as the "overweighted", but affordable relative to lithium, and lithium was assumed to rule the high energy density market in the time to come. This allegory is however misleading, as it came at the anode side with a fatal intellectual dependence on the concept of graphite intercalation, which for sodium, restricts capacity, rate, and lifetime, at this moment in a nonacceptable fashion. It was partly ignored that sodium is in fact chemically very different: due to the fact that the cohesion energy density of sodium is by a factor of 0.36 smaller than that of Li; nucleation, wetting, and surface interactions are more easy to control for Na by materials design, so that sodium batteries in fact, offer some additional and even more effective modes of energy storage, beyond intercalation. This comparison between "Li@C_6" (372 mAh g^{-1}) and "Na@C" (potentially up to 1000 mAh g^{-1}) makes us very optimistic that the race for the next battery system (cheaper, more sustainable, and more performing) is not decided, but rather open.

Acknowledgements

Conflict of Interest

The authors declare no conflict of interest.

Keywords

[1] S. Chu, Y. Cui, N. Liu, *Nat. Mater.* **2017**, *16*, 16.
[2] D. Larcher, J.-M. Tarascon, *Nat. Chem.* **2015**, *7*, 19.
[3] B. Dunn, H. Kamath, J.-M. Tarascon, *Science* **2011**, *334*, 928.
[4] Y. Zhong, X. Xu, P. Liu, R. Ran, S. P. Jiang, H. Wu, Z. Shao, *Adv. Enegy Mater.* **2020**, *10*, 2002992.
[5] Y. Zhang, Z. Lyu, Z. Chen, S. Zhu, Y. Shi, R. Chen, M. Xie, Y. Yao, M. Chi, M. Shao, Y. Xia, *Angew. Chem., Int. Ed.* **2021**, *133*, 19795.
[6] M. Li, J. Lu, Z. Chen, K. Amine, *Adv. Mater.* **2018**, *30*, 1800561.
[7] Y. Zhang, H. Wang, Z. Luo, H. T. Tan, B. Li, S. Sun, Z. Li, Y. Zong, Z. J. Xu, Y. Yang, K. A. Khor, Q. Yan, *Adv. Energy Mater.* **2016**, *6*, 1600453.
[8] Y. Shi, J. Wan, J.-Y. Li, X.-C. Hu, S.-Y. Lang, Z.-Z. Shen, G. Li, H.-J. Yan, K.-C. Jiang, Y.-G. Guo, *Nano Energy* **2019**, *61*, 304.
[9] B. Li, B. Xi, Z. Feng, Y. Lin, J. Liu, J. Feng, Y. Qian, S. Xiong, *Adv. Mater.* **2018**, *30*, 1705788.
[10] C. Delmas, *Adv. Energy Mater.* **2018**, *8*, 1703137.
[11] Y. Zhang, W. Liu, T. Wang, Y. Du, Y. Cui, S. Liu, H. Wang, S. Liu, M. Chen, J. Zhou, *Adv. Mater. Interfaces* **2020**, *7*, 2000953.
[12] J. Park, M. Lee, D. Feng, Z. Huang, A. C. Hinckley, A. Yakovenko, X. Zou, Y. Cui, Z. Bao, *J. Am. Chem. Soc.* **2018**, *140*, 10315.
[13] G. Fang, Z. Wu, J. Zhou, C. Zhu, X. Cao, T. Lin, Y. Chen, C. Wang, A. Pan, S. Liang, *Adv. Energy Mater.* **2018**, *8*, 1703155.
[14] Y. Chen, X. Li, K. Park, W. Lu, C. Wang, W. Xue, F. Yang, J. Zhou, L. Suo, T. Lin, H. Huang, J. Li, J. B. Goodenough, *Chem* **2017**, *3*, 152.
[15] J. Ding, H. Wang, Z. Li, A. Kohandehghan, K. Cui, Z. Xu, B. Zahiri, X. Tan, E. M. Lotfabad, B. C. Olsen, D. Mitlin, *ACS Nano* **2013**, *7*, 11004.
[16] L. Li, Y. Zheng, S. Zhang, J. Yang, Z. Shao, Z. Guo, *Energy Environ. Sci.* **2018**, *11*, 2310.
[17] H. Fatima, Y. Zhong, H. Wu, Z. Shao, *Mater. Rep. Energy* **2021**, *1*, 100022.
[18] Y. Zhang, W. Sun, Z.-Z. Luo, Y. Zheng, Z. Yu, D. Zhang, J. Yang, H. T. Tan, J. Zhu, X. Wang, *Nano Energy* **2017**, *40*, 576.
[19] Y. Zheng, Y. Wang, Y. Lu, Y.-S. Hu, J. Li, *Nano Energy* **2017**, *39*, 489.
[20] X. Xiang, K. Zhang, J. Chen, *Adv. Mater.* **2015**, *27*, 5343.
[21] M.-S. Balogun, Y. Luo, W. Qiu, P. Liu, Y. Tong, *Carbon* **2016**, *98*, 162.
[22] B. Jache, J. O. Binder, T. Abe, P. Adelhelm, *Phys. Chem. Chem. Phys.* **2016**, *18*, 14299.
[23] H. Kim, J. Hong, Y. U. Park, J. Kim, I. Hwang, K. Kang, *Adv. Funct. Mater.* **2015**, *25*, 534.
[24] M. Goktas, C. Bolli, E. J. Berg, P. Novák, K. Pollok, F. Langenhorst, M. v. Roeder, O. Lenchuk, D. Mollenhauer, P. Adelhelm, *Adv. Energy Mater.* **2018**, *8*, 1702724.
[25] A. Ponrouch, A. Goñi, M. R. Palacín, *Electrochem. Commun.* **2013**, *27*, 85.
[26] D. Stevens, J. Dahn, *J. Electrochem. Soc.* **2000**, *147*, 1271.
[27] P. Thomas, D. Billaud, *Electrochim. Acta* **2002**, *47*, 3303.
[28] H. Hou, X. Qiu, W. Wei, Y. Zhang, X. Ji, *Adv. Energy Mater.* **2017**, *7*, 1602898.

[29] C. M. Ghimbeu, J. Górka, V. Simone, L. Simonin, S. Martinet, C. Vix-Guterl, *Nano Energy* **2018**, *44*, 327.

[30] Y. Zhang, L. Li, Y. Xiang, G. Zou, H. Hou, W. Deng, X. Ji, *ACS Appl. Mater. Interfaces* **2020**, *12*, 30431.

[31] Q. Jin, W. Li, K. Wang, H. Li, P. Feng, Z. Zhang, W. Wang, K. Jiang, *Adv. Funct. Mater.* **2020**, *30*, 1909907.

[32] W. Chen, M. Wan, Q. Liu, X. Xiong, F. Yu, Y. Huang, *Small Methods* **2019**, *3*, 1800323.

[33] P. Barpanda, L. Lander, S. i. Nishimura, A. Yamada, *Adv. Energy Mater.* **2018**, *8*, 1703055.

[34] H. Li, M. Xu, Z. Zhang, Y. Lai, J. Ma, *Adv. Funct. Mater.* **2020**, *30*, 2000473.

[35] F. Yu, L. Du, G. Zhang, F. Su, W. Wang, S. Sun, *Adv. Funct. Mater.* **2020**, *30*, 1906890.

[36] Y. Xiao, N. M. Abbasi, Y. F. Zhu, S. Li, S. J. Tan, W. Ling, L. Peng, T. Yang, L. Wang, X. D. Guo, *Adv. Funct. Mater.* **2020**, *30*, 2001334.

[37] Y. E. Durmus, H. Zhang, F. Baakes, G. Desmaizieres, H. Hayun, L. Yang, M. Kolek, V. Küpers, J. Janek, D. Mandler, *Adv. Energy Mater.* **2020**, *10*, 2000089.

[38] X. L. Xu, K. San Hui, D. A. Dinh, K. N. Hui, H. Wang, *Mater. Horiz.* **2019**, *6*, 1306.

[39] Y. C. Liu, Y. Li, H. Y. Kang, T. Jin, L. F. Jiao, *Mater. Horiz.* **2016**, *3*, 402.

[40] Y. P. Deng, Z. G. Wu, R. Liang, Y. Jiang, D. Luo, A. Yu, Z. Chen, *Adv. Funct. Mater.* **2019**, *29*, 1808522.

[41] M. Á. Muñoz-Márquez, D. Saurel, J. L. Gómez-Cámer, M. Casas-Cabanas, E. Castillo-Martínez, T. Rojo, *Adv. Energy Mater.* **2017**, *7*, 1700463.

[42] Z. Tian, N. Chui, R. Lian, Q. Yang, W. Wang, C. Yang, D. Rao, J. Huang, Y. Zhang, F. Lai, C. Liu, T. Liu, *Energy Storage Mater.* **2020**, *27*, 591.

[43] J. Huang, J. Wang, R. Xie, Z. Tian, G. Chai, Y. Zhang, F. Lai, G. He, C. Liu, T. Liu, P. R. Shearing, D. J. L. Brett, *J. Mater. Chem. A* **2020**, *8*, 19879.

[44] J. Huang, Y. Li, R. Xie, J. Li, Z. Tian, G. Chai, Y. Zhang, F. Lai, G. He, C. Liu, T. Liu, D. J. L. Brett, *J. Energy Chem.* **2020**, *58*, 147.

[45] B. Cao, X. Li, *Acta Phys.-Chim. Sin.* **2020**, *36*, 1905003.

[46] Y. Li, Y. S. Hu, M. M. Titirici, L. Chen, X. Huang, *Adv. Energy Mater.* **2016**, *6*, 1600659.

[47] J. Yang, Z. Ju, Y. Jiang, Z. Xing, B. Xi, J. Feng, S. Xiong, *Adv. Mater.* **2018**, *30*, 1700104.

[48] Z. Hong, Y. Zhen, Y. Ruan, M. Kang, K. Zhou, J. M. Zhang, Z. Huang, M. Wei, *Adv. Mater.* **2018**, *30*, 1802035.

[49] X. Chen, Y. Zheng, W. Liu, C. Zhang, S. Li, J. Li, *Nanoscale* **2019**, *11*, 22196.

[50] B. Xiao, T. Rojo, X. Li, *ChemSusChem* **2018**, *12*, 133.

[51] B. Guo, J. Shu, K. Tang, Y. Bai, Z. Wang, L. Chen, *J. Power Sources* **2008**, *177*, 205.

[52] L. Xiao, H. Lu, Y. Fang, M. L. Sushko, Y. Cao, X. Ai, H. Yang, J. Liu, *Adv. Energy Mater.* **2018**, *8*, 1703238.

[53] D. Sun, D. Luo, B. Wang, Y. Tang, X. Ji, L. Wang, *Nano Energy* **2019**, *64*, 103937.

[54] K.-L. Hong, L. Qie, R. Zeng, Z.-Q. Yi, W. Zhang, D. Wang, W. Yin, C. Wu, Q.-J. Fan, W.-X. Zhang, *J. Mater. Chem. A* **2014**, *2*, 12733.

[55] K. Kim, D. G. Lim, C. W. Han, S. Osswald, V. Ortalan, J. P. Youngblood, V. G. Pol, *ACS Sustainable Chem. Eng.* **2017**, *5*, 8720.

[56] L. Yang, M. Hu, Q. Lv, H. Zhang, W. Yang, R. Lv, *Carbon* **2020**, *163*, 288.

[57] N. Zhang, Q. Liu, W. Chen, M. Wan, X. Li, L. Wang, L. Xue, W. Zhang, *J. Power Sources* **2018**, *378*, 331.

[58] A. Adamson, R. Väli, M. Paalo, J. Aruväli, M. Koppel, R. Palm, E. Härk, J. Nerut, T. Romann, E. Lust, *RSC Adv.* **2020**, *10*, 20145.

[59] T. Zhang, J. Mao, X. Liu, M. Xuan, K. Bi, X. L. Zhang, J. Hu, J. Fan, S. Chen, G. Shao, *RSC Adv.* **2017**, *7*, 41504.

[60] Z. Lin, Q. Xia, W. Wang, W. Li, S. Chou, *InfoMat* **2019**, *1*, 376.

[61] M. E. Lee, S. M. Lee, J. Choi, D. Jang, S. Lee, H. J. Jin, Y. S. Yun, *Small* **2020**, *16*, 2001053.

[62] D. Saurel, B. Orayech, B. Xiao, D. Carriazo, X. Li, T. Rojo, *Adv. Energy Mater.* **2018**, *8*, 1703268.

[63] D. Stevens, J. Dahn, *J. Electrochem. Soc.* **2000**, *147*, 4428.

[64] D. Stevens, J. Dahn, *J. Electrochem. Soc.* **2001**, *148*, A803.

[65] S. Komaba, W. Murata, T. Ishikawa, N. Yabuuchi, T. Ozeki, T. Nakayama, A. Ogata, K. Gotoh, K. Fujiwara, *Adv. Funct. Mater.* **2011**, *21*, 3859.

[66] B. Zhang, C. M. Ghimbeu, C. Laberty, C. Vix-Guterl, J. M. Tarascon, *Adv. Energy Mater.* **2016**, *6*, 1501588.

[67] P. Bai, Y. He, X. Zou, X. Zhao, P. Xiong, Y. Xu, *Adv. Energy Mater.* **2018**, *8*, 1703217.

[68] L. Fu, K. Tang, K. Song, P. A. van Aken, Y. Yu, J. Maier, *Nanoscale* **2014**, *6*, 1384.

[69] J. Liu, H. Liu, T. Yang, G. Wang, M. O. Tade, *Chin. Sci. Bull.* **2014**, *59*, 2186.

[70] S. Qiu, L. Xiao, M. L. Sushko, K. S. Han, Y. Shao, M. Yan, X. Liang, L. Mai, J. Feng, Y. Cao, X. Ai, H. Yang, J. Liu, *Adv. Energy Mater.* **2017**, *7*, 1700403.

[71] Y. Cao, L. Xiao, M. L. Sushko, W. Wang, B. Schwenzer, J. Xiao, Z. Nie, L. V. Saraf, Z. Yang, J. Liu, *Nano Lett.* **2012**, *12*, 3783.

[72] A. Gomez-Martin, J. Martinez-Fernandez, M. Ruttert, M. Winter, T. Placke, J. Ramirez-Rico, *Chem. Mater.* **2019**, *31*, 7288.

[73] Q. Deng, F. Chen, S. Liu, A. Bayaguud, Y. Feng, Z. Zhang, Y. Fu, Y. Yu, C. Zhu, *Adv. Funct. Mater.* **2020**, *30*, 1908665.

[74] Z. Zhu, F. Liang, Z. Zhou, X. Zeng, D. Wang, P. Dong, J. Zhao, S. Sun, Y. Zhang, X. Li, *J. Mater. Chem. A* **2018**, *6*, 1513.

[75] H. Lu, F. Ai, Y. Jia, C. Tang, X. Zhang, Y. Huang, H. Yang, Y. Cao, *Small* **2018**, *14*, 1802694.

[76] S. Alvin, H. S. Cahyadi, J. Hwang, W. Chang, S. K. Kwak, J. Kim, *Adv. Energy Mater.* **2020**, *10*, 2000283.

[77] B. H. Hou, Y. Y. Wang, Q. L. Ning, W. H. Li, X. T. Xi, X. Yang, H. J. Liang, X. Feng, X. L. Wu, *Adv. Mater.* **2019**, *31*, 1903125.

[78] Y. Jin, S. Sun, M. Ou, Y. Liu, C. Fan, X. Sun, J. Peng, Y. Li, Y. Qiu, P. Wei, *ACS Appl. Energy Mater.* **2018**, *1*, 2295.

[79] S. Alvin, D. Yoon, C. Chandra, H. S. Cahyadi, J.-H. Park, W. Chang, K. Y. Chung, J. Kim, *Carbon* **2019**, *145*, 67.

[80] X. Dou, I. Hasa, D. Saurel, C. Vaalma, L. Wu, D. Buchholz, D. Bresser, S. Komaba, S. Passerini, *Mater. Today* **2019**, *23*, 87.

[81] D. Ni, W. Sun, Z. Wang, Y. Bai, H. Lei, X. Lai, K. Sun, *Adv. Energy Mater.* **2019**, *9*, 1900036.

[82] A. Agrawal, S. Janakiraman, K. Biswas, A. Venimadhav, S. Srivastava, S. Ghosh, *Electrochim. Acta* **2019**, *317*, 164.

[83] M. Letellier, F. Chevallier, M. Morcrette, *Carbon* **2007**, *45*, 1025.

[84] R. Yan, E. Josef, H. Huang, K. Leus, M. Niederberger, J. P. Hofmann, R. Walczak, M. Antonietti, M. Oschatz, *Adv. Funct. Mater.* **2019**, *29*, 1902858.

[85] Y. Lu, Y. Lu, Z. Niu, J. Chen, *Adv. Energy Mater.* **2018**, *8*, 1702469.

[86] Y. Zhang, X. Xia, B. Liu, S. Deng, D. Xie, Q. Liu, Y. Wang, J. Wu, X. Wang, J. Tu, *Adv. Energy Mater.* **2019**, *9*, 1803342.

[87] K. Schutjajew, T. Tichter, J. Schneider, M. Antonietti, C. Roth, M. Oschatz, *Phys. Chem. Chem. Phys.* **2021**, *23*, 11488.

[88] H. Au, H. Alptekin, A. C. Jensen, E. Olsson, C. A. O'Keefe, T. Smith, M. Crespo-Ribadeneyra, T. F. Headen, C. P. Grey, Q. Cai, *Energy Environ. Sci.* **2020**, *13*, 3469.

[89] N. Sun, Z. Guan, Y. Liu, Y. Cao, Q. Zhu, H. Liu, Z. Wang, P. Zhang, B. Xu, *Adv. Energy Mater.* **2019**, *9*, 1901351.

[90] J. M. Stratford, P. K. Allan, O. Pecher, P. A. Chater, C. Grey, *Chem. Commun.* **2016**, *52*, 12430.

[91] Z. Tian, N. Fechler, M. Oschatz, T. Heil, J. Schmidt, S. Yuan, M. Antonietti, *J. Mater. Chem. A* **2018**, *6*, 19013.

[92] R. Walczak, B. Kurpil, A. Savateev, T. Heil, J. Schmidt, Q. Qin, M. Antonietti, M. Oschatz, *Angew. Chem., Int. Ed.* **2018**, *57*, 10765.

2102489 (16 of 17)

[93] B. Sun, P. Li, J. Zhang, D. Wang, P. Munroe, C. Wang, P. H. Notten, G. Wang, *Adv. Mater.* **2018**, *30*, 1801334.

[94] D. Xie, J. Zhang, G. Pan, H. Li, S. Xie, S. Wang, H. Fan, F. Cheng, X. Xia, *ACS Appl. Mater. Interfaces* **2019**, *11*, 18662.

[95] X. Zheng, P. Li, Z. Cao, W. Luo, F. Sun, Z. Wang, B. Ding, G. Wang, Y. Huang, *Small* **2019**, *15*, 1902688.

[96] B. Sun, P. Li, J. Zhang, D. Wang, P. Munroe, C. Wang, P. H. L. Notten, G. Wang, *Adv. Mater.* **2018**, *30*, 1801334.

[97] R. Yan, M. Antonietti, M. Oschatz, *Adv. Energy Mater.* **2018**, *8*, 1800026.

[98] Z. Tian, F. Lai, T. Heil, S. Cao, M. Antonietti, *Sci. China Mater.* **2020**, *63*, 748.

[99] W. Liu, P. Liu, D. Mitlin, *Chem. Soc. Rev.* **2020**, *49*, 7284.

[100] Z. W. Seh, J. Sun, Y. Sun, Y. Cui, *ACS Cent. Sci.* **2015**, *1*, 449.

[101] L. Chen, R. Yan, M. Oschatz, L. Jiang, M. Antonietti, K. Xiao, *Angew. Chem., Int. Ed.* **2020**, *59*, 9067.

[102] H. Wang, Y. Shao, S. Mei, Y. Lu, M. Zhang, J. K. Sun, K. Matyjaszewski, M. Antonietti, J. Yuan, *Chem. Rev.* **2020**, *120*, 9363.

[103] M. Antonietti, M. Oschatz, *Adv. Mater.* **2018**, *30*, 1706836.

[104] Z. Pan, J. Ren, G. Guan, X. Fang, B. Wang, S. G. Doo, I. H. Son, X. Huang, H. Peng, *Adv. Energy Mater.* **2016**, *6*, 1600271.

[105] J. Yang, X. Zhou, D. Wu, X. Zhao, Z. Zhou, *Adv. Mater.* **2017**, *29*, 1604108.

[106] M. Yu, Z. Yin, G. Yan, Z. Wang, H. Guo, G. Li, Y. Liu, L. Li, J. Wang, *J. Power Sources* **2020**, *449*, 227514.

[107] S. Alvin, C. Chandra, J. Kim, *Chem. Eng. J.* **2020**, *391*, 123576.

[108] M. Hu, L. Yang, K. Zhou, C. Zhou, Z.-H. Huang, F. Kang, R. Lv, *Carbon* **2017**, *122*, 680.

[109] F. Wu, L. Liu, Y. Yuan, Y. Li, Y. Bai, T. Li, J. Lu, C. Wu, *ACS Appl. Mater. Interfaces* **2018**, *10*, 27030.

[110] K. Yu, H. Zhao, X. Wang, M. Zhang, R. Dong, Y. Li, Y. Bai, H. Xu, C. Wu, *ACS Appl. Mater. Interfaces* **2020**, *12*, 10544.

[111] L. Ye, M. Liao, T. Zhao, H. Sun, Y. Zhao, X. Sun, B. Wang, H. Peng, *Angew. Chem., Int. Ed.* **2019**, *131*, 17210.

[112] Z. Zheng, X. Zeng, H. Ye, F. Cao, Z. Wang, *ACS Appl. Mater. Interfaces* **2018**, *10*, 30417.

[113] C. Chu, N. Wang, L. Li, L. Lin, F. Tian, Y. Li, J. Yang, S.-X. Dou, Y. Qian, *Energy Storage Mater.* **2019**, *23*, 137.

[114] A. Susca, J. Liu, J. Cui, N. Mubarak, J. Wu, M. Ihsan-Ul-Haq, F. Ciucci, J.-K. Kim, *J. Mater. Chem. A* **2020**, *8*, 14757.

[115] F. Wu, J. Zhou, R. Luo, Y. Huang, Y. Mei, M. Xie, R. Chen, *Energy Storage Mater.* **2019**, *22*, 376.

[116] P. Liu, Y. Wang, Q. Gu, J. Nanda, J. Watt, D. Mitlin, *Adv. Mater.* **2020**, *32*, 1906735.

[117] H. Au, H. Alptekin, A. C. S. Jensen, E. Olsson, C. A. O'Keefe, T. Smith, M. Crespo-Ribadeneyra, T. F. Headen, C. P. Grey, Q. Cai, A. J. Drew, M.-M. Titirici, *Energy Environ. Sci.* **2020**, *13*, 3469.

[118] K. Tang, L. Fu, R. J. White, L. Yu, M.-M. Titirici, M. Antonietti, J. Maier, *Adv. Energy Mater.* **2012**, *2*, 873.

[119] Z. Tian, N. López-Salas, C. Liu, T. Liu, M. Antonietti, *Adv. Sci.* **2020**, *7*, 2001767.

[120] Z. Tian, T. Heil, J. Schmidt, S. Cao, M. Antonietti, *ACS Appl. Mater. Interfaces* **2020**, *12*, 13127.

Zhihong Tian is a professor of the Henan University. She obtained her first Ph.D. degree in engineering at the Zhengzhou University in 2018, and a second Ph.D. degree in natural science at the Potsdam University in 2019 in Germany. After finishing her Ph.D. studies, she worked as a postdoctoral assistant at the Max Planck Institute of Colloids and Interfaces. In January 2021, she joined the Engineering Research Center for Nanomaterials of Henan University. Her research interests lie in the design and synthesis of porous polymer and carbon materials for gas separation, energy storage, and conversion.

Markus Antonietti is a Director of the Max Planck Institute of Colloids and Interfaces. He published around 900 papers in the fields of polymers, materials chemistry, sustainable chemistry, and energy materials. In his free time, he likes gardening, cooking, and playing in a rock band.